ANALYZING SPACE-BASED INTERFEROMETRIC

MEASUREMENTS OF STARS and NETWORK MEASUREMENTS

OF GAMMA-RAY BURSTS

L. G. Taff
Department of Physics and Astronomy
The Johns Hopkins University
3400 North Charles Street
Baltimore, MD 21218

The attached pre-print represents the summary of the work prepared under this NASA Grant and is in concordance with the work proposed to be funded by this Grant. For gamma-ray bursts in particular, experimental capabilities have finessed the need for this work.

GAMMA-RAY BURST ASTROMETRY V:

ERROR BOXES FOR THE ATTEIA *ET AL.* CATALOG

L. G. Taff
Department of Physics and Astronomy
The Johns Hopkins University
3400 North Charles Street
Baltimore, MD 21218

ABSTRACT

Since the announcement of the discovery of sources of bursts of gamma-ray radiation in 1973, hundreds more reports of such bursts have now been published. Numerous artificial satellites have been equipped with gamma-ray detectors including the very successful Compton Gamma Ray Observatory BATSE instrument. Unfortunately, we have made no progress in identifying the source(s) of this high energy radiation. We suspected that this was a consequence of the method used to define gamma-ray burst source "error boxes." An alternative procedure to compute gamma-ray burst source positions, with a purely physical underpinning, was proposed in 1988 by Taff. Since then we have also made significant progress in understanding the analytical nature of the triangulation problem and in computing actual gamma-ray burst positions and their corresponding error boxes. For the former, we can now mathematically illustrate the crucial role of the area occupied by the detectors, while for the latter, the Atteia *et al.* (1987) catalog has been completely re-reduced. There are very few discrepancies in locations between our results and those of the customary "time difference of arrival" procedure. Thus, we have numerically demonstrated that the end result, for the positions, of these two very different-looking procedures is the same. Finally, for the first time, we provide a sample of realistic "error boxes" whose non-simple shapes vividly portray the difficulty of burst source localization.

Subject Headings: gamma rays: bursts—astrometry

1. BACKGROUND AND INTRODUCTION

An alternative to the customary "time difference of arrival" method of gamma-ray burst source location was presented by Taff in 1988. In the new algorithm, for any number of detectors, all their locations and times of observation are folded into a single, straightforward computation. Thus, unlike the former method, this technique predicts a unique location for the source of the burst independent of the number of different gamma-ray sensors registering the burst (once there are more than three of them). In contrast, for each pair of detectors, the standard method only defines a (circular) locus of points on the celestial sphere on which the burst source location resides. When there are more than three recordings of the same burst, then the "time difference of arrival" procedure specifies a pair of intersections [as does the new method in this case which also analytically subsumes it; see Taff (1988a)]. As more independent detections are added the older technique delineates a finite area on the celestial sphere via a pair-wise analysis of the location and timing data. With real data— and with a very difficult problem of time registration of bursts observed with devices of different responsivities and sensitivities, timing errors arising from recording the photons in discrete temporal bins, differing thresholds before recording is initiated, spacecraft location and clock errors, and so forth—the geometrically pure problem is degraded into one whose best possible outcome is that all the intersection points lie near each other. This area has been used to define an "error-box" in which the burst source is believed to lie (see Fig. 1).

Unfortunately, the position deduced in this fashion will, in general, not necessarily be the statistically most likely place for the source of the burst. The hope that the circle drawn for each pair of detecting sensors is centered in a region of high source location probability can not be consistently realized in practice; indeed, the circle must lie completely outside a "one-sigma" error region fairly often. Furthermore, since no detailed computation of a probabilistically rigorous region surrounding the most probable source location circle has ever been published or described in the literature, the issue of systematic effects are even less clear because the underlying probability function may not be well-behaved. One could

compute the one-sigma regions in an attempt to produce reliable error estimates as, for instance, Pizzichini (1981) has suggested. However, none have been published heretofore. Moreover, the amount of computation necessary for the customary method must exceed that necessary to similarly characterize the results of Taff's (1988a) method by the ratio of (number of points in a circle):one since this is the ratio of their prediction volumes. Hence, such a calculation for the time difference of arrival technique would be unwieldy and extremely expensive in terms of the quantity of numerical work required. Moreover, when one does make error boxes based on the results of Taff's algorithm, the "error boxes" are frequently not *boxes* at all as can be seen in the many figures shown below. A more complete comparison between the different aspects of the two methods was given in Table 1 of Taff & Holfeltz (1992a).

The technique developed in Taff (1988a) is easily amenable to numerical simulation. Extensive Monte Carlo computations of its predictions for the position of gamma-ray bursts are summarized in Taff & Holfeltz (1992a,b) and Taff, Scott & Holfeltz (1993). Those calculations explored ranges of numbers of potential spacecraft-carrying burst detectors in cislunar (2, 3, or 4) and interplanetary (1, 2, 3, or 4) space, and all 4π steradians of potential burst source positions. In sum, they conclusively show that this method can routinely achieve a minute of arc prediction precision and accuracy, for realistic random errors, once there are two interplanetary spacecraft in the burst detection network. Non-random errors or very large fortuituous errors represent untried circumstances in simulation. The reason for the minimum number of detectors constraint is that the area occupied by the sensors is the key to a well-determined solution. This will be mathematically demonstrated below.

Before briefly reviewing the fundamental ideas behind this method, we address an apparent deficiency of the initial formulation of the problem; namely that it was a monochromatic construct. As some of the difficulties we face when attempting to delineate the positions of gamma-ray bursts have to do with the different responsivities and sensitivities of the various detectors, we can not be certain that recorded photon arrival times from different sensors

represent the same phenomena, in a temporal sense, within the burst structure. However, this difficulty is an inherent part of gamma-ray burst observing. In any case this complication, for one energy band, is not severe for we can always imagine that the quantity T defined in Eq. (3) below is part of the integrand in an integral over frequency. The other element of the integrand would be the spectral energy distribution of the source multiplied by the response function of the detector. Because the latter function is relatively sharply peaked, the integral approximately reduces to the product of the other two terms, each evaluated at the effective wavelength, multiplied by the energy passband width. These factors are phase independent and only result in an unimportant re-normalization of T. Hence, the monochromatic formulation for one detector is appropriate.

Unfortunately this generalization can not be easily extended to cover widely separated wavelength bands both because the above mentioned mathematical approximations rapidly degrade and, more importantly, without an explicit model for the mechanism of the gamma-ray burst, one has to make a strong assumption regarding the temporal evolution of the burst over all observed frequencies. This compounds, when it is not the origin of, the trying problem with regard to systematic errors in the timing and no merely statistical adjustment technique is going to overcome it.

Below we more fully explicate the underlying mathematical structure of the technique (see also Taff, Scott & Holfeltz 1993). In particular, we have discovered that the general (*i.e.*, $N > 3$) co-planar case is exactly solvable. Indeed, it is trivial to do so analytically—the equations for the source position vector direction cosines are two linear equations in two unknowns. Hence, for instance, because the timing errors dominate this problem we could explicitly compute the error distributions for the source position direction cosines from those posited for the spacecraft-to-spacecraft timings. Moreover, since the real case is nearly co-planar, additional, approximate, numerical experiments are now very easy to perform. Furthermore, as the ideal case is so close to the actual situation, we now have both

an excellent starting guess and the key to constructing a robust numerical solution algorithm for the general situation. This is discussed, along with its one limitation, in §3.1.

In some instances the three dimensionality of the detector configuration is important or the orientation of the burst source wave front vector is nearly co-planar with the constellation of observing spacecraft. When either situation occurs an alternative starting point is required. We have created one and to use it we have to compute our initial guess based on the restriction that the number of sensors is only three (see §3.2). However, for most gamma-ray bursts recorded by more than three detectors, the redundant satellites will be in cislunar space rather than in interplanetary space. As it is the *area* occupied by the sensors which is most important to precisely determining the burst source location—rather than their number—this is of no real consequence (§2.2). We first find the triplet of detectors which occupy the most area and then compute an estimate for the direction based on the timings from these three (which are necessarily co-planar). A straightforward algorithm based on Heron's formula for the area of a triangle is presented in §2.2. This computation can be exactly performed following, for instance, Pizzichini (1981).

Finally, using our software an entirely new catalog of burst source locations, for every gamma-ray burst in the Atteia *et al.* catalog (1987) for which we have the observational data, has been re-computed. Moreover, each new source location is described herein by a reliable error estimate given the applicability of the spacecraft location errors and the spacecraft-to-spacecraft timing errors (§4). These include "error boxes" calculated as Pizzichini (1981) suggested.

2. THE BASIC CONCEPT

The essential physical concept behind our technique was to use the one piece of information about the gamma-ray burst that we indisputedly know (Taff 1988b); to wit, that the phase of the burst (whether planar or spherical as would be the case for solar bursts) is an invariant for all detectors. Could the recording devices on the spacecraft of the interplanetary burst network measure the phase ϕ of the burst wave front, then they would all obtain the same value (absent observational errors of course) namely,

$$\phi = \mathbf{k} \cdot \mathbf{r} - \omega t \qquad (1)$$

where $\mathbf{r}$ is the solar system barycentric location of the spacecraft, t is the time of arrival of the burst at that spacecraft, $\mathbf{k}$ is the wave vector of the burst wave front, and ω is the angular frequency of the (assumed monochromatic) burst ($= 2\pi\nu$ where ν is the frequency of the photon; $\nu = c/\lambda$ where c is the speed of light in vacuo and λ is the wavelength of the burst). Rewriting $\mathbf{k}$ as $k\mathbf{u}$, where $\mathbf{u}$ is the wave front normal, the pseudo-invariant Φ can be defined, viz.

$$\Phi = \mathbf{u} \cdot \mathbf{r} - ct. \qquad (2)$$

Although neither ϕ nor Φ can be directly measured, they do include all the observational data at our disposal *and* the quantity we want to determine; namely $\mathbf{u}$. Taff (1988a) proposed that, especially in the presence of unknown systematics and the very difficult time registration problem we have in gamma-ray burst observing, enforcing the constraint that each sensor's (albeit unknown and unmeasurable) value of Φ be the same would lead to a mathematically well-posed problem for the computation of $\mathbf{u}$. The method used was to minimize the quantity

$$T = (1/2) \sum_{n,m=1}^{N} (\Phi_n - \Phi_m)^2 \qquad (3)$$

subject to the constraint that $\mathbf{u} \cdot \mathbf{u} = 1$. By explicit computation, Taff (1988a) further showed that the customary time of arrival analysis was contained in this principle as a special case of minimizing Eq. (3) (*i.e.*, it is represented by the cases of $N = 2$ and $N = 3$). Finally, Taff

also explicitly computed the co-planar solution for u when N was equal to 4. We now show that this result can be generalized to any number of co-planar sensors.

2.1. $N > 3$ and Co-planar

To see how this result can be generalized to any number of co-planar sensors write u as u $= (\alpha, \beta, \gamma)$ and use two of the three direction cosines as the independent variables. That is, substitute for one of the direction cosines, say γ, in terms of the other two, and regard T as a function of the two (now) independent variables α and β. In other words, since $\alpha^2 + \beta^2 + \gamma^2 = 1$ then

$$\gamma = \gamma(\alpha,\beta) = \pm(1 - \alpha^2 - \beta^2)^{1/2} \tag{4}$$

so

$$T(\alpha,\beta) = (1/2) \sum_{n=1}^{N} \sum_{m=1}^{N} (\Phi_n - \Phi_m)^2. \tag{5}$$

where

$$\Phi = \alpha x + \beta y + \gamma(\alpha,\beta)z - ct.$$

The ambiguity in the square root for gamma in Eq. (4) shows the analytical origins of the bi-directionality uncertainty associated with the case of co-planar detectors.

Now let the plane $z = 0$ be the plane of the ecliptic. If the detectors are in this plane, then all the gamma-dependent terms disappear in Eq. (5) because they were all multiplied by the z coordinate of one of the detectors and these have been all hypothesized to be equal to zero. In other words, the problem of finding the minimum value for T is reduced to the system of equations $\nabla_{\mathbf{u}} T|_{z=0} = 0$, or

$$\partial T/\partial \alpha|_{z=0} = \sum_{n=1}^{N} \sum_{m=1}^{N} (\Phi_n - \Phi_m)|_{z=0}(x_n - x_m) = 0,$$

$$\partial T/\partial \beta|_{z=0} = \sum_{n=1}^{N} \sum_{m=1}^{N} (\Phi_n - \Phi_m)|_{z=0}(y_n - y_m) = 0,$$

with Φ now reduced to $\Phi|_{z=0} = \alpha x + \beta y - ct$. But these are just two linear, inhomogeneous equations in the two unknowns alpha and beta. Hence, the solution is trivial to obtain (all sums go from 1 to N),

$$\alpha = D^{-1} \begin{vmatrix} \sum X_{nm}\tau_{nm} & \sum X_{nm}Y_{nm} \\ \sum Y_{nm}\tau_{nm} & \sum Y_{nm}^2 \end{vmatrix}, \qquad \beta = D^{-1} \begin{vmatrix} \sum X_{nm}^2 & \sum X_{nm}\tau_{nm} \\ \sum X_{nm}Y_{nm} & \sum Y_{nm}\tau_{nm} \end{vmatrix}, \qquad (6a)$$

with the determinant of the system D given by

$$D = \begin{vmatrix} \sum X_{nm}^2 & \sum X_{nm}Y_{nm} \\ \sum X_{nm}Y_{nm} & \sum Y_{nm}^2 \end{vmatrix}. \qquad (6b)$$

We have represented the spacecraft-to-spacecraft relative location vector as $\mathbf{R}_{nm} = \mathbf{r}_n - \mathbf{r}_m$ and the spacecraft-to-spacecraft burst arrival relative time, in linear measure, as $\tau_{nm} = c(t_n - t_m)$.

2.2. An Areal Interpretation for D

The areal distribution of the sensors plays a crucial role in the solvability of the problem (*i.e.*, D must not vanish else the system of equations would be linearly dependent) and in the stability of the solution (*e.g.*, $|D|$ should be of non-negligible norm so that D^{-1} is well-defined). Although numerically clear from our application of Cramer's rule, we shall also illustrate this—in a geometrically transparent fashion—immediately below.

First consider the case of $N = 3$ necessarily co-planar detectors. Using the determinant form for the area of a triangle with vertices at (x_1, y_1), (x_2, y_2), and (x_3, y_3), viz.

$$\text{area} = A = (1/2) \begin{vmatrix} x_1 & y_1 & 1 \\ x_2 & y_2 & 1 \\ x_3 & y_3 & 1 \end{vmatrix}, \qquad (7)$$

one can show, by some straightforward algebra, that D in Eq. (6b) is exactly equal to $48A^2$. Thus, we have an explicit proof that, when N is equal to 3, our geometrical intuition is a good guide; the larger the area of the triangle occupied by the three spacecraft the larger the value of the determinant of the system which led to Eqs. (6a) and, therefore, the more stable its numerical solution. Clearly this reasoning also holds for the case of only 2 sensors in that the vanishing of D implies that the source can not be localized. Indeed, as mentioned

in §1, it was known from other considerations that when N was 2 only a small circle on the sky could be delineated as the origin of the burst.

If we try to generalize this result beyond $N = 3$, for instance when $N = 4$ by exploiting the fact that the area of any quadrilateral is the sum of the areas of the two triangles which comprise it, then we will fail. One can explicitly show that when N is 4, D is no longer equal to *any* quadratic function of the area of the spacecraft quadrilateral. Nonetheless, there is an interpretation of D in the general (*i.e.*, $N > 3$) co-planar case which also simply reflects on our ability to solve for the burst wave front direction, the numerical stability of the solution, and the distribution of the detectors.

To see this meaning for D, imagine that instead of dealing with D in the ecliptic coordinate system as above, while remaining in the plane of the ecliptic we first rotate to principal axis coordinates (say u and v) of the spacecraft configuration [*i.e.*, we find the coordinate system which will make the moment of inertia tensor of the system diagonal (assuming equal masses for the spacecraft)]. In this coordinate system the off-diagonal elements of D will be zero (by construction) and $|D|$ itself will be explicitly reduced to the product of its eigenvalues. Moreover, in the principal axis coordinate system the eigenvalues of this matrix are the variances of the rectangular coordinates u and v (for the mean values of u and v can be first made to vanish via an in-plane translation). Thus, $|D| = \sigma_u^2 \sigma_v^2$ will be large and the solution for the unit normal to the burst wave front well-determined and numerically stable, precisely when the distribution of the spacecraft is such to maximize their "spread." So, no matter how large N is, a nearly collinear constellation of spacecraft (*i.e.*, one principal axis variance σ_u or σ_v nearly equal to zero) would not be able to produce a good estimate for the position of a gamma-ray burst.

2.3. Analytical Error Estimates

To see that the error distributions for α and β are simple to compute from those of τ, and thence the timings $\{t_n\}$, re-examine Eqs. (6). Tau and the times of observation only

appear in the numerator of the expressions for α and β and therein they do so linearly. Thus, with the assumption of any reproductive error distribution for the timing errors, those of the independent direction cosines alpha and beta are immediately obtainable. Whether or not such simplistic assumptions are justifiable is a separate question. The linearity of the functional relationship among α, β, and τ assures us that more generally the distribution of the τ_{nm} follows from that of t_n and t_m via a convolution.

3. AN ALGORITHM FOR THE NON-CO-PLANAR CASE

3.1. Use of the General Co-planar Solution

Assume that our coordinate system is the solar system, barycentric, rectangular ecliptic one. Also relax the assumption that the N spacecraft are co-planar. Then the complete partial derivatives of T with respect to α and β are given by

$$\partial T/\partial \alpha = \sum_{n=1}^{N} \sum_{m=1}^{N} (\Phi_n - \Phi_m)[x_n - x_m - (\alpha/\gamma)(z_n - z_m)] = 0,$$
$$\partial T/\partial \beta = \sum_{n=1}^{N} \sum_{m=1}^{N} (\Phi_n - \Phi_m)[y_n - y_m - (\beta/\gamma)(z_n - z_m)] = 0. \tag{8}$$

Most of the $|z_n|$, $n = 1, 2, 3, \ldots, N$ will be small compared to 1 A.U. because of the nearness of the spacecraft to the plane of the ecliptic. Therefore, the multipliers of the explicit alpha and beta terms will usually be numerically small. Thus, we can envision the following successive substitution iteration procedure. First assume that the detectors are in the plane of the ecliptic. Solve for the direction cosines of u using Eqs. (6a) and (6b). Next compute the value of gamma from Eq. (4). There will be two values, owing to the two branches of the square root in Eq. (4). Call them $\gamma_\pm$. Pick one sign, say the minus sign for now. Then re-compute the values for (what we will now refer to as) α_- and β_-. Perform this calculation utilizing the full derivatives of T, but by regarding the linear z dependent terms in Eqs. (8) as fixed. That is, re-write Eqs. (8) as

$$\sum_{n=1}^{N} \sum_{m=1}^{N} (\Phi_n - \Phi_m)(x_n - x_m) = (\alpha/\gamma) \sum_{n=1}^{N} \sum_{m=1}^{N} (\Phi_n - \Phi_m)(z_n - z_m),$$
$$\sum_{n=1}^{N} \sum_{m=1}^{N} (\Phi_n - \Phi_m)(y_n - y_m) = (\beta/\gamma) \sum_{n=1}^{N} \sum_{m=1}^{N} (\Phi_n - \Phi_m)(z_n - z_m), \tag{9}$$

with α and β on the right hand side known quantities, their values given by the last stage in the iteration process. The next step in the iteration procedure is to re-define γ_- from Eq. (4) with the negative sign, solve the inhomogeneous linear system given in Eqs. (9) anew for the values of α_- and β_-, and so on until convergence is achieved. The last phase of the

computation is to initially choose the other sign for gamma and repeat the entire iterative solution process just described all over again. $T_- = T(\alpha_-, \beta_-)$ and $T_+ = T(\alpha_+, \beta_+)$ can be evaluated from Eq. (5). The one which is the smaller, when N is greater than 3, tells us which choice of sign for the square root was correct.

At one stage in our work we had mistakenly thought that using the amplitude of T might also work for the case of only 3 sensors. This is wrong; in fact, we have been able to analytically demonstrate that the value of T is exactly zero at its minimum when N is equal to 3. Numerically of course, the electronic digital computer finds some very small value and the logic we implemented to choose the smallest between $T_\pm$ does so but without any mathematical or physical content. When N exceeds 3 the magnitude of T *does* carry information though a constellation of nearly collinear spacecraft or a group of nearly co-planar spacecraft also lying in the plane containing the direction of the burst can lead to uncertainty (see the figures below).

The source of the last remark lies in the structure of Eqs. (9); one instance wherein this procedure might not be numerically stable is when the norm of γ is very small. In this instance the rest of the quantities on the right hand sides in Eq. (9) will be multiplied by a relatively large value potentially inducing either a runaway (if the first values are not especially accurate) or an oscillation between two fixed points. We have observed both types of behavior in our numerical experiments with the latter occurring much more frequently than the former. Of course if $|\gamma|$ is small then the burst wave front unit normal nearly lies in the plane of the sensors, hence one's inability to precisely determine the (small) out-of-plane component. In these instances there is another alternative starting value which we can pursue.

3.2. Use of the N = 3 Solution

First let us recount the analytical solution to the three-dimensional, $N = 3$ problem published by Pizzichini (1981) as re-formulated in Taff (1988a):

$$\mathbf{u} = A\mathbf{R}_{21} + B\mathbf{R}_{31} + C\mathbf{R}_{31} \times \mathbf{R}_{21}, \qquad (10a)$$

where A, B, and C are given by

$$A|\mathbf{R}_{31} \times \mathbf{R}_{21}|^2 = \tau_{21} R_{31}^2 - \tau_{31} \mathbf{R}_{31} \cdot \mathbf{R}_{21}, \qquad (10b)$$

$$B|\mathbf{R}_{31} \times \mathbf{R}_{21}|^2 = \tau_{31} R_{31}^2 - \tau_{21} \mathbf{R}_{31} \cdot \mathbf{R}_{21}, \qquad (10c)$$

and

$$C^2|\mathbf{R}_{31} \times \mathbf{R}_{21}|^2 = 1 - A^2 R_{21}^2 - B^2 R_{31}^2 - 2AB\mathbf{R}_{31} \cdot \mathbf{R}_{21}. \qquad (10d)$$

Note that the uncertainty in the sign of γ in Eq. (4) has been replaced, in this form of the solution, by the uncertainty in the sign of C. Finally, this is equivalent to the solution given in Eqs. (6) after a rotation from the north pole of the ecliptic to the direction of the z axis of the original coordinate system.

To see how we can use this representation of u as a starting guess for the general problem, we use Heron's formula for the area of a triangle, viz.

$$\text{area} = [s(s - a)(s - b)(s - c)]^{1/2},$$

where the semi-perimeter s is given by $(a + b + c)/2$ in terms of the lengths of the sides of the triangle a, b, and c. Since we have rectangular coordinate system coordinates for the locations of the detectors, we may compute the lengths of the sides from the Pythagorean theorem. Determining the maximum area subset from $N > 3$ spacecraft is now simply an enumeration problem. (As there is an analog of Heron's theorem for quadrilaterals, one might conjecture that expanding this to polygons of more sides would be beneficial. Unfortunately, four points need not be co-planar so that finding the first value for u would be as difficult as finding the ultimate value for u.)

The alternative procedure to follow for $N > 3$ sensors is simple: (1) Find the maximum area triplet of the N spacecraft carrying the gamma-ray detectors. (2) Use the A, B, C formulation for u given in Eqs. (10) to find a first approximation to the direction to the source. Since C is uncertain as to sign, this provides two possible bearings. (3) Set up the general (*i.e.*, $N > 3$) phase discrepancy minimization problem which is a pair of non-linear equations in the two unknowns α and β, namely Eqs. (8). (4) Solve this set using as a starting value the solution in step #2. Repeat for the other sign of C and choose the one which minimizes T. The result is the value of u we seek.

4. THE RE-REDUCTION OF THE ATTEIA *ET AL.* CATALOG

We have upgraded our Monte Carlo software to work on the real data behind the Atteia *et al.* (1987) catalog kindly supplied to us by K. Hurley. In general, as predicted in Taff (1988a), we obtain the same results for $N = 3$ although there are some minor discrepancies. *The same statement is also true for $N > 3$.* Our new results are in Tables 1 and 2 along with the original Atteia *et al.* (1987) answers. Table 1 includes those bursts for which we were supplied 3 observations; Table 2 is for those for which we have more than 3 observations. Assuming normal distributions of both spacecraft and timing errors, based on the information in the files supplied to us, the "error boxes" for these cases are in Figs. 2–46.

The error boxes shown in the figures were computed as follows: We followed Pizzichini's (1981) suggestion that the timing and the spacecraft errors are normally distributed about zero means. (No referee would allow anything else.) From the data files generously furnished by K. Hurley, we had relative timing and coordinate errors. When the error information was incomplete, we took the *maximum* relative timing error for all other pairs of detectors. These values were used as standard deviations about the mean in a conventional, electronic digital computer, normally distributed random number generator. One million samples were obtained for every scatter diagram we plot and the gamma-ray burst position deduced by the methods discussed above. The figures were then constructed.

Two different types of phenomena are clear in the figures; the anticipated, localized box-like structure and non-box-like structure. The former tend to validate the simplistic assumptions heretofore asserted. However, even in some $N > 4$ cases, there are two boxes illustrating the two-fold uncertainty in the γ or C square root discussed above. At first we thought that one box might originate from taking one sign for the square root and the other box from the other sign but this is not the case. Solutions from both signs appear in both boxes. There is a marked preference, typically 80%/20%, for only one box and the preferred one is that which the software chose to be the solution to the overall problem. The existence, in the Monte Carlo simulations only, of a continued ambiguity for the place of origin of the

gamma-ray bursts apparently depends on some subtle numerical bifurcation to which the placement problem is sensitive.

The non-box-like structure is sometimes just an elongated box [see Fig. 3] but more frequently very different, topologically, from anything we could reasonably describe as a "box." This was predicted as a consequence of the role of the systematic errors. Even though we have only used the normal distribution to generate the Monte Carlo samples, the systematic errors are already embedded in the measurements. For instance, the long and narrow boxes aligned along one equatorial coordinate axis explain the largest discrepancies between our results and the Atteia *et al.* positions. In these instances the error is almost all in one of the equatorial coordinates and the customary time difference of arrival method has landed in a slightly different position along what is essentially a narrow arc. The more interesting shapes combined with the projection effects again point to further subtleties in the gamma-ray astrometry problem.

6. SUMMARY

As the Burst And TranSiEnt instrument on the Compton Gamma Ray Observatory satellite has clearly shown us, gamma-ray bursts are daily events and they are isotropically distributed on the celestial sphere. This means that they are either very close to us or very far away from us. Simplicity, and some energy arguments, compel us to come to the conclusion that these are not solar neighborhood events. Hence, even if the gamma-ray emitting objects are quite faint, at all wavelengths, in their quiescent state, the fact that no gamma-ray burst source has been positively identified may not mean that we have been looking in the wrong places (*e.g.*, witness the optical discovery of the Geminga x-ray source). We believe that in this and our previous papers we have shown that we know how to compute where the optimum places are and how to attach realistic errors to these positions.

Acknowledgements

Table 1. Our Gamma-Ray Burster coordinates versus Atteia *et al.* 1987 results.

					Three Detectors			
	Our		Our	Alternate	Atteia *et al.*		Atteia *et al.*	Alternate
Burst ID	RA	DEC	RA	DEC	RA	DEC	RA	DEC
B780914	97.51	54.99	94.35	−8.31	97.5	55.		
B780918	250.79	40.57	183.51	−75.51	241.	40.5		
B781006.B	2.09	13.42	11.27	−7.62	2.1	13.4		
B781012.A	159.53	18.86	152.47	1.19	160.	19.	270.	−17.
B781019	177.89	−15.51	190.06	12.05	177.9	−15.5	238.	37.
B781023	207.07	6.62	194.26	−24.14	211.	4.		
B781025	120.39	−22.95	151.01	57.82	42.	−15.5		
B781026	261.14	3.48	256.28	−49.60	261.	3.5		
B781102.A	232.33	−9.31	227.23	−27.37	232.	−9.	183.	9.
B781217	236.38	10.93	217.71	−46.60	236.	11.	210.	−39.
B790101	183.54	15.45	170.93	−13.04	183.	15.		
B790105	209.11	−24.83	217.49	−2.03	209.	−25	226.	9.
B790107	271.38	−23.87	271.37	−23.01	271.	−24.		
B790116	158.04	−12.96	174.61	24.80	158.	−13.		
B790119	251.56	−22.35	251.56	−22.38	250.	−21.		
B790208	138.89	−58.70	224.92	56.44	324.5	39.5		
B790211	133.82	−7.92	150.51	38.02	142.7	7.4		
B790213	310.08	10.20	328.70	−42.13	310.1	10.2		
B790305.A	42.18	−22.16	12.29	45.38	34.8	−5.2	12.3	45.4
B790327.B	198.00	−59.54	236.78	28.34	208.	−35.5	236.8	28.3

Table 1. *Continued.*

	Our		Our	Alternate	Atteia *et al.*		Atteia *et al.*	Alternate
Burst ID	RA	DEC	RA	DEC	RA	DEC	RA	DEC
B790412.B	92.64	−11.59	94.94	58.40	93.2	−5.2		
B790504	347.80	31.90	17.60	−29.48	347.8	31.9		
B790514	37.65	60.75	65.29	−22.23	37.7	60.7		
B790622.B	325.63	−37.49	311.11	5.10	325.6	−41.4		
B790929	93.49	23.40	93.49	23.42	87.5	30.		
B791014	94.83	−37.00	122.76	82.87	96.3	−34.6		
B791018	220.33	−31.99	229.68	−2.22	220.34	−31.99	230.05	−3.23
B791031.A	254.89	−82.32	267.54	35.67	254.9	−82.3		
B791105	243.21	38.99	182.43	−69.48	251.2	24.3		
B791111	215.80	−36.20	229.03	3.38	213.9	−33.7	229.04	3.4
B791215	51.49	51.50	66.80	−10.32	51.5	51.5		
B791220.A	74.63	−60.92	292.08	69.95	74.61	−60.91	299.22	66.63
B791222.A	6.99	10.18	12.18	−1.91	7.0	10.15	16.5	−7.9
B800103.A	29.83	−34.44	349.50	43.31	29.82	−34.43	349.53	34.37
B800105	15.44	2.95	12.83	9.14	13.1	7.6		
B800116	187.25	16.73	172.35	−16.56	180.	0.5		
B800213	104.54	−15.35	118.56	59.59	104.5	−15.3	−	

Table 2. Our Gamma-Ray Burster coordinates versus Atteia *et al.* 1987 results.

Four or More Detectors

Burst ID	Our		Atteia *et al.*	
	RA	DEC	RA	DEC
B780921	132.70	34.55	132.6	34.4
B781115.A	210.37	52.13	210.8	52.2
B781121.A	255.64	0.86	255.8	0.6
B790402.B	122.61	−50.39	122.6	−50.4
B790419	334.68	−41.97	334.7	−42.0
B790731	101.64	26.66	101.3	22.5
B791101	292.36	41.01	294.6	38.1
B791115	211.64	23.82	211.	24.3

REFERENCES

Atteia, J.-L., Barat, C., Hurley, K., Niel, M., Vedienne, G., Evans, W. D., Ferimore, E. E., Klebesadel, R. W., Laros, J. G., Cline, T., Desai, U., Teegarden, B., Estulin, I. V., Zenchenko, V. M., Kuznetsou, A. V. & Kurt, V. G. 1987, ApJ Suppl 64, 305

Pizzichini, G. 1981, Adv. Space Res. 1, 227

Taff, L. G. 1988a, ApJ 326, 1032

Taff, L. G. 1988b, Phys. Rev. 37A, 4943

Taff, L. G. & Holfeltz, S. T. 1992a, Proceedings of the Compton Observatory Science Workshop, eds. C. R. Shrader, N. Gehrels, and B. Dennis, NASA Conf. Publ. 3137, pg. 301

Taff, L. G. & Holfeltz, S. T. 1992b, Proceedings of the Huntsville Gamma-Ray Workshop, eds. W. S. Paciesas and G. J. Fishman, AIP Conf. Proc. 265, pg. 378

Taff, L. G., Scott, J. H. & Holfeltz, S. T. 1993, in Proceedings of the Compton Gamma-Ray Observatory Conference, eds. M. Friedlander, N. Gehrels, and D. J. Macomb, AIP Conf. Proc. 280, pg. 818

FIGURE LEGENDS

Figure 1. General intersection area for "time difference of arrival" gamma-ray burst source location determination. Note that the error bands need not be symmetrically placed relative to the circular locus nor include the most probable circle.

Figure 2. Distribution on 1,000,000 samples in a Monte Carlo simulation for the position of gamma ray burst B780914. In this case there are two areas of intense distribution, associated with the higher probability regions deriving from the two square root branches, a filled in pair of arcs joining them (at this high level of simulation the appearance is one of continuity), and what we believe to be an portion of an arc orthogonal to the curve joining the two highest probability points. Only by pushing the Monte Carlo process to the extreme, and sampling improbable error values, can the full structure be revealed.

Figure 3. The B780918 burst location region. While it looks like there ought to be a symmetrically placed other half as in the previous figure, there is not. We have no analytical explanation, as yet, for features such as this or the ones in the previous figure. They will turn out to be fairly common.

Figure 4. The 1,000,000 Monte Carlo simulation pattern for the B780921 burst. In this case we have something approaching an error "box," essentially a long arc whose width derives from the uncertainty in the error estimate. Note that the burst site itself is not well-localized.

Figure 5a. The B781006.B burst locus. The darkened points in the middle are printer malfunctions.

Figure 5b. An expansion of one of the regions in the previous figure showing that the box is really an extended rectangle.

Figure 6. One of our favorites, the B781012.A figure. The regions of maximum probability are clearly visible because of the higher density of points as is the orthogonal axis set crossing through these zones. This is another feature which will turn out to be common but only visible if the full range of possible errors is explored. The thin arcs in between the regions of highest probability are similar to those seen in Fig. 2.

Figure 7a. The more usual two elongated box structure one expects to originate from the two branches of the square root; this time for a million sample distribution for B781019.

Figure 7b. An expanded view of the more southerly high likelihood region.

Figure 8. A unique picture, that for B781023. It shows two symmetric well-defined regions of a high probability—albeit not well-localized—with the orthogonally symmetrical arc clearly visible.

Figure 9. The B781025 burst scatter diagram which is very similar to that of B780918 in Fig. 3.

Figure 10. The B781026 plot showing two distinctly separate regions and the same type of localized perpendicular structure first seen in Fig. 6.

Figure 11. An example showing both the localized normal features through the regions of maximum probability and the arc orthogonal to the curve joining the two regions of most likely location. The relative thinness of the localized perpendicular feature in this case is unexplained. This is for the B781102.A burst.

Figure 12a. The 1,000,000 scatter diagram for the B781115.A gamma-ray burst.

Figure 12b. An expanded version of the more northerly high probability locality in the previous diagram. The parallel horizontal structure is real and not an artifact of the plotting package or hardware. It will occur in later pictures too. An unlikely interpretation is that it reflects the periodic aspects of the random number generator.

Figure 13. A second lined structure graph, this time for the B781121.A burst.

Figure 14. The B781217 plot similar to that in Fig. 2. The difference in apparent ellipticity is a consequence of the difference in inclination of the orbital plane of the three detectors to that of the celestial equator.

Figure 15. The B790101 diagram showing poorly localized positions on long arcs of high probability.

Figure 16. A by now familiar picture for the B790105 burst. The use of a rectangular projection of the celestial sphere makes the claim that the thin arc is perpendicular to the curve joining the two regions of highest probability clearer in this case.

Figure 17. Another one-sided burst, this is for B790107.

Figure 18. A more complex version of the scatter diagram first seen in Fig. 6. Once again, the projection effects of the plane of the three detectors with respect to the celestial equator makes the image more difficult to interpret. This is for B790116 gamma-ray burst.

Figure 19. A remarkable picture, that for B790119.

Figure 20. Another extreme diagram, again because of projection effects, for the B790208 burst. The two regions of high probability are clearly visible as is the essentially continuous connection between them (because of the extensive sampling). In addition, the non-local orthogonal arc segments are visible too.

Figure 21. The B790211 burst scatter diagram. The non-local normal arc is clearly visible. We believe that the tight loops represent one facet of the simulation and that the wider, fuzzy regions are the orthogonal facet more clearly seen in previous figures.

Figure 22. The B790213 figure, showing all the features we believe to be present in the previous diagram, but more clearly because of the different circumstances of projection.

Figure 23. The locus of possible points for the B790305.A burst. Once again we see the two high likelihood expanses, the local orthogonal fuzzy areas, the connecting bands, and the displaced perpendicular strip. The points near 60 deg declination and 360 deg (i.e., 24 hours) right ascension represent wrap-around in this rectangular projection of the celestial sphere.

Figure 24. The B790327.B pattern similar to ones we have seen before.

Figure 25. Another familiar illustration, this time for the B790402.B gamma-ray burst.

Figure 26. The well-separated, but not well-localized, high probability areas for the B790412.B burst. The crossing structure shows the local perpendicular structure seen in high perspective.

Figure 27. The two square root branch structure for the B790419 burst.

Figure 28a. Extreme separation in the case of the B790504 burst.

Figure 28b. An expanded view of the more southerly locus of preferred locations showing a well-localized burst and something we could honestly term an error "box."

Figure 29. The locus of high probability points for the B790514 burst.

Figure 30. The pattern for the B790622.B burst.

Figure 31. Another example of the parallel line structure, in this case to the declination axis, for the B790731 burst.

Figure 32. A replication of Fig. 2, in essence, for the B790929 burst.

Figure 33. The B791014 scatter diagram of high probability points.

Figure 34. The B791018 well-separated and well-localized burst location possibilities from the two branches of the square root.

Figure 35. Another burst with the localized orthogonal crossing pattern; this time for B791031.A.

Figure 36a. The B791101 burst source locus with wrap-around at the vernal-equinox for the more southerly possibility.

Figure 36b. An expanded view of the northerly locus in the previous plot showing a real error box.

Figure 37. The B791105 plot which shows no small scale structure because of the large scale of the diagram.

Figure 38. The B791111 burst locus.

Figure 39. The scatter diagram for the B791115 gamma-ray burst. Once again the hint of the joining bridge is visible but projection effects have masked the locally orthogonal region (if it is present).

Figure 40. The B791215 burst source position locus.

Figure 41. The well-separated and well-localized pair of high probability areas for the B791220.A burst.

Figure 42. Another clear view of the two higher probability regions, their locally orthogonal counterparts of markedly different width (though projection effects are important in this plot), and the separate perpendicular arc (B791222.A).

Figure 43. The B800103.A burst locus.

Figure 44. A nice representation of the filling in effect between the two high probability regions and the separated orthogonal arc. For the B800105 burst.

Figure 45. Essentially the same plot as the previous one but with a less clear separation. We do not know if this is real or a relic of the relative projections involved. For the B800116 gamma-ray burst.

Figure 46. The B800213 burst locus pattern.

True Circle #1

Actual Source Location

"Error Box"

True Circle #2

Error Contaminated Circle #2 Plus 1σ Band

Error Contaminated Circle #1 Plus 1σ Band

B780914

RIGHT ASCENSION (deg)

DECLINATION (deg)

B780918

DECLINATION (deg)

RIGHT ASCENSION (deg)

B780921

B781006.B

RIGHT ASCENSION (deg)

DECLINATION (deg)

B781006.B

B781012.A

DECLINATION (deg)

RIGHT ASCENSION (deg)
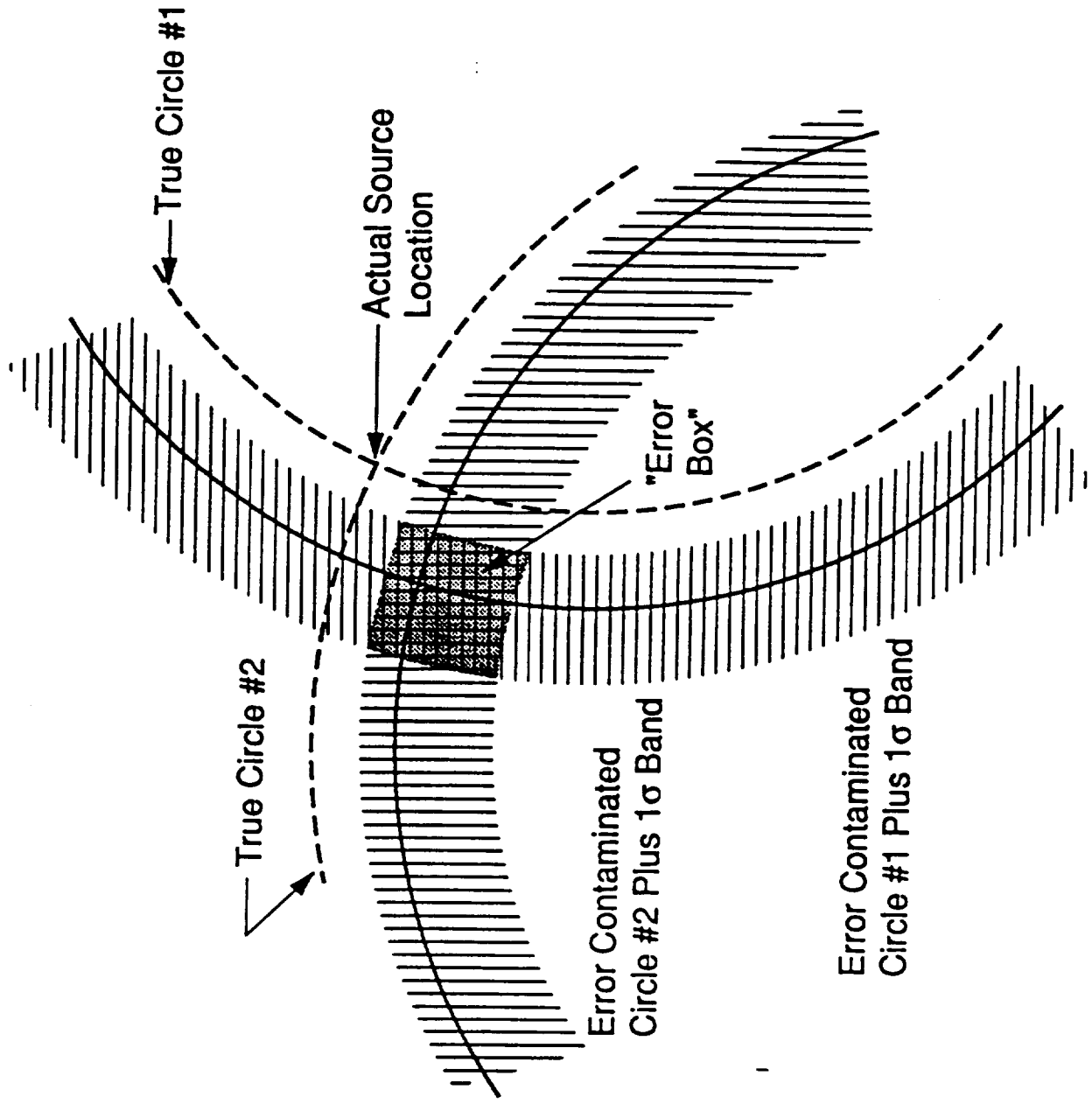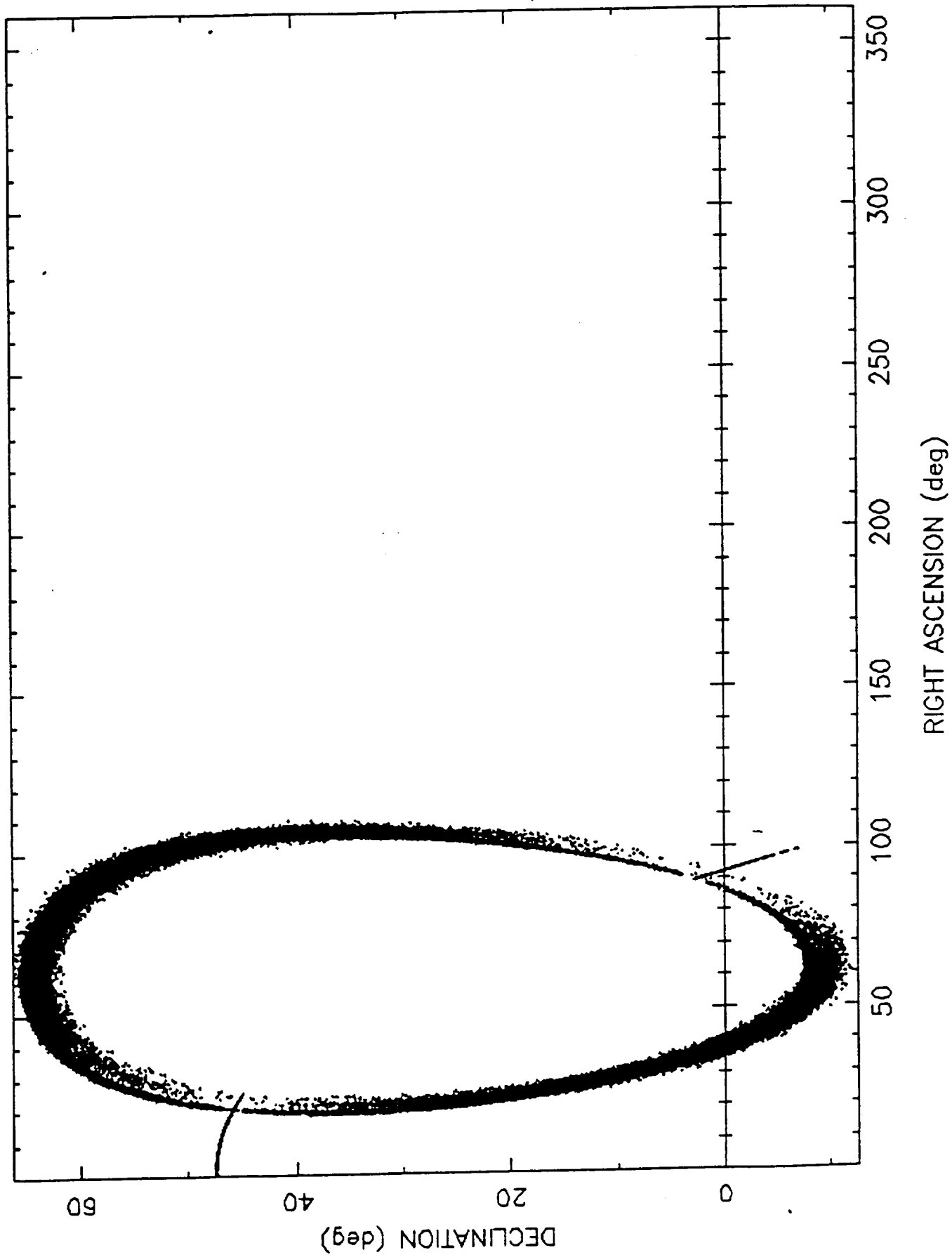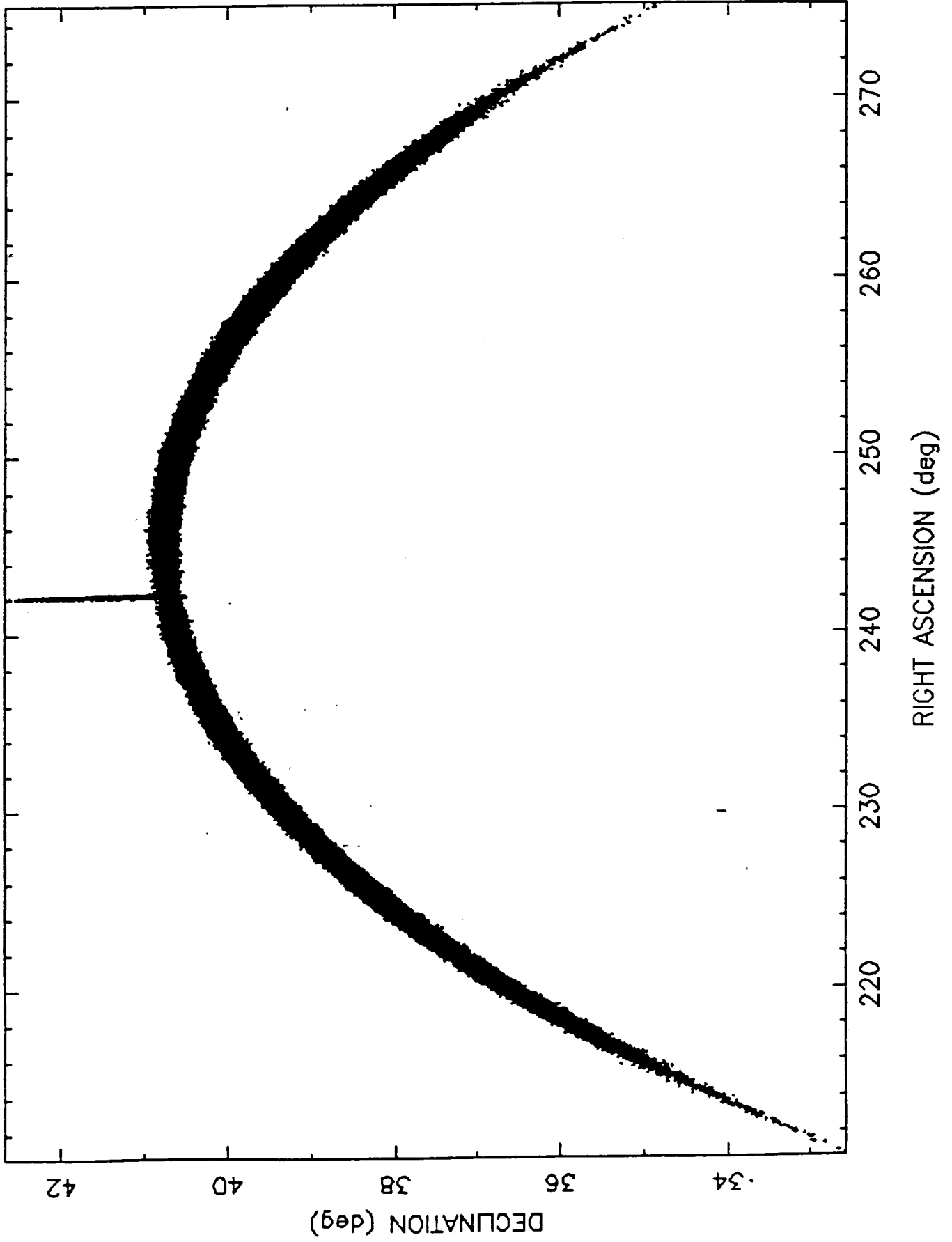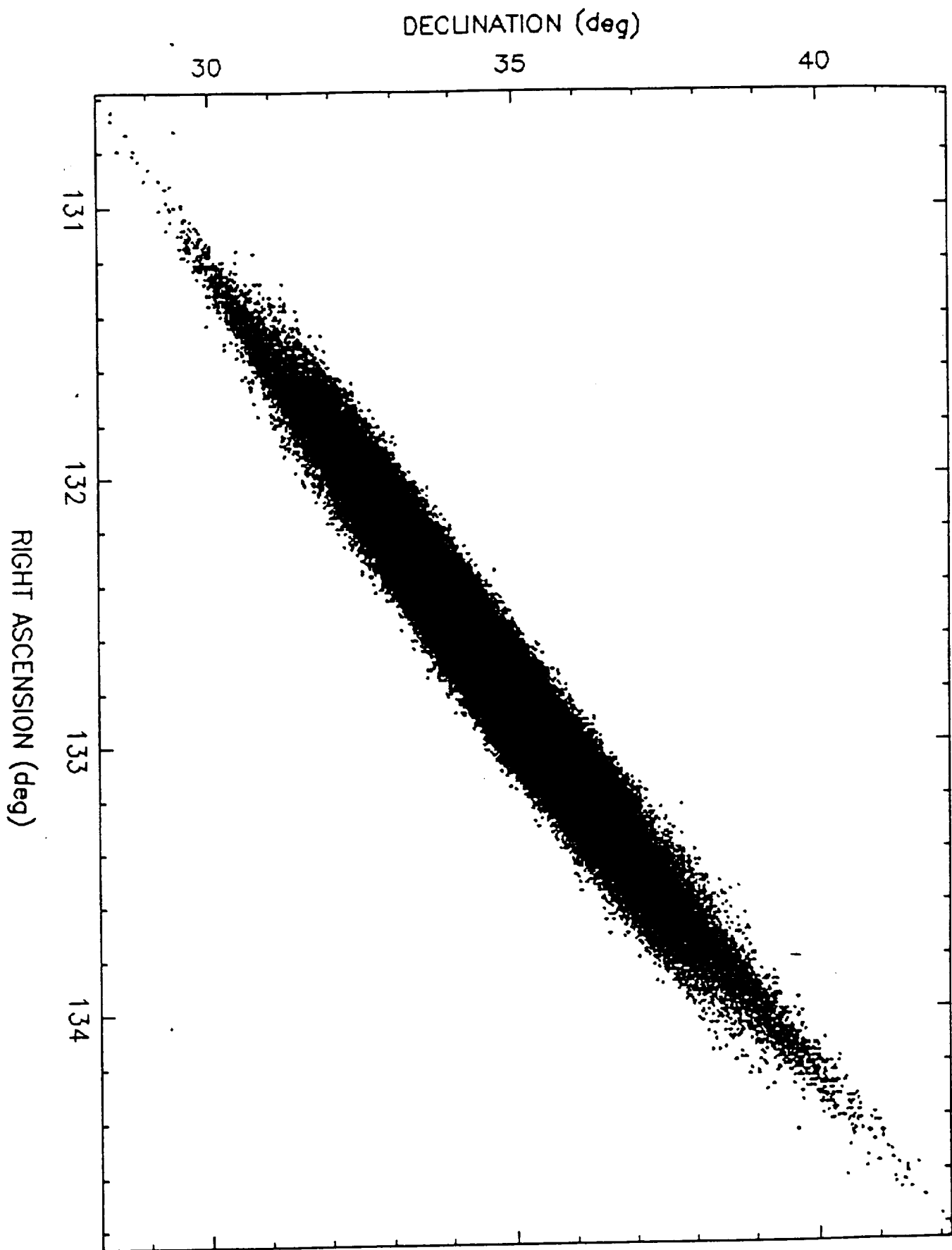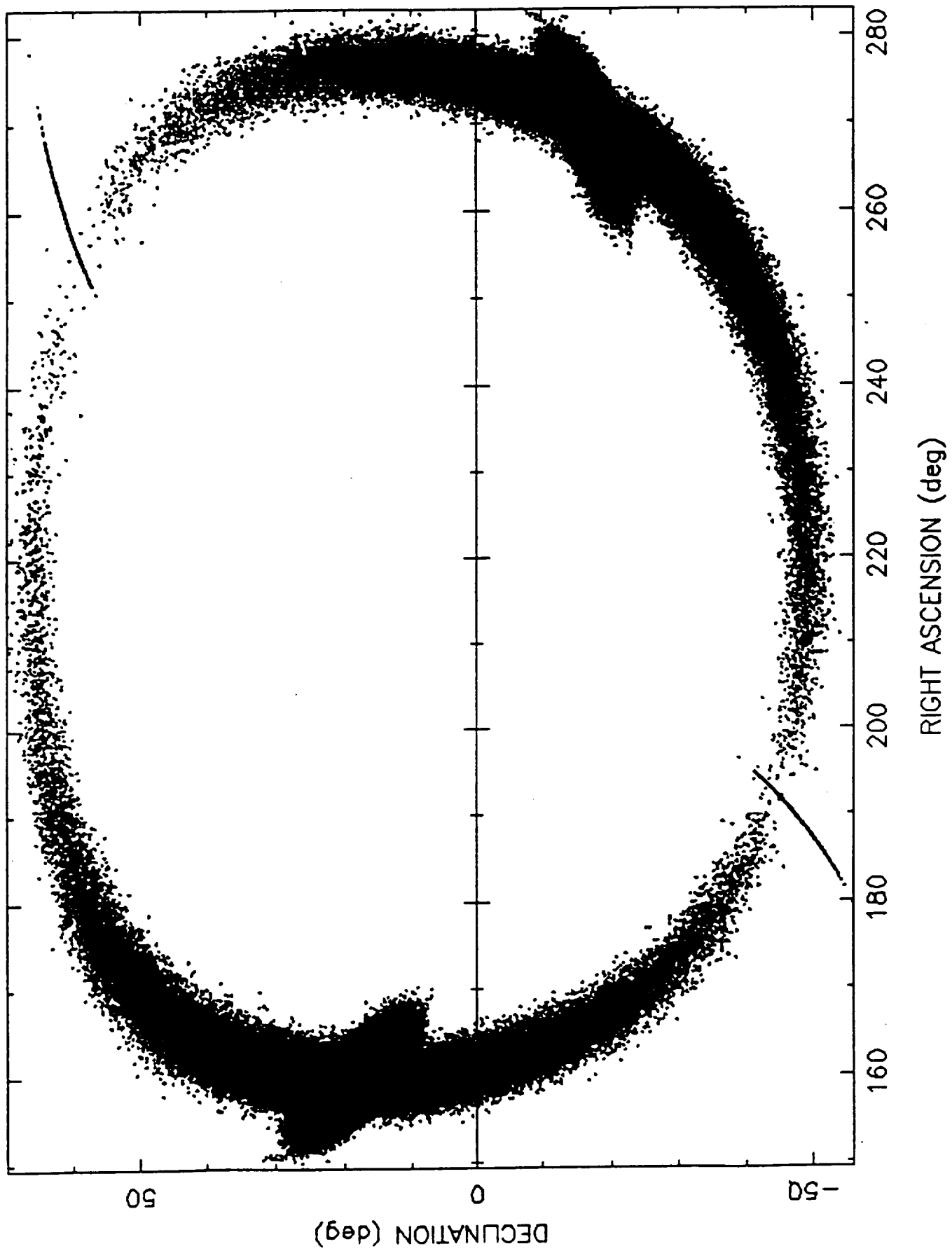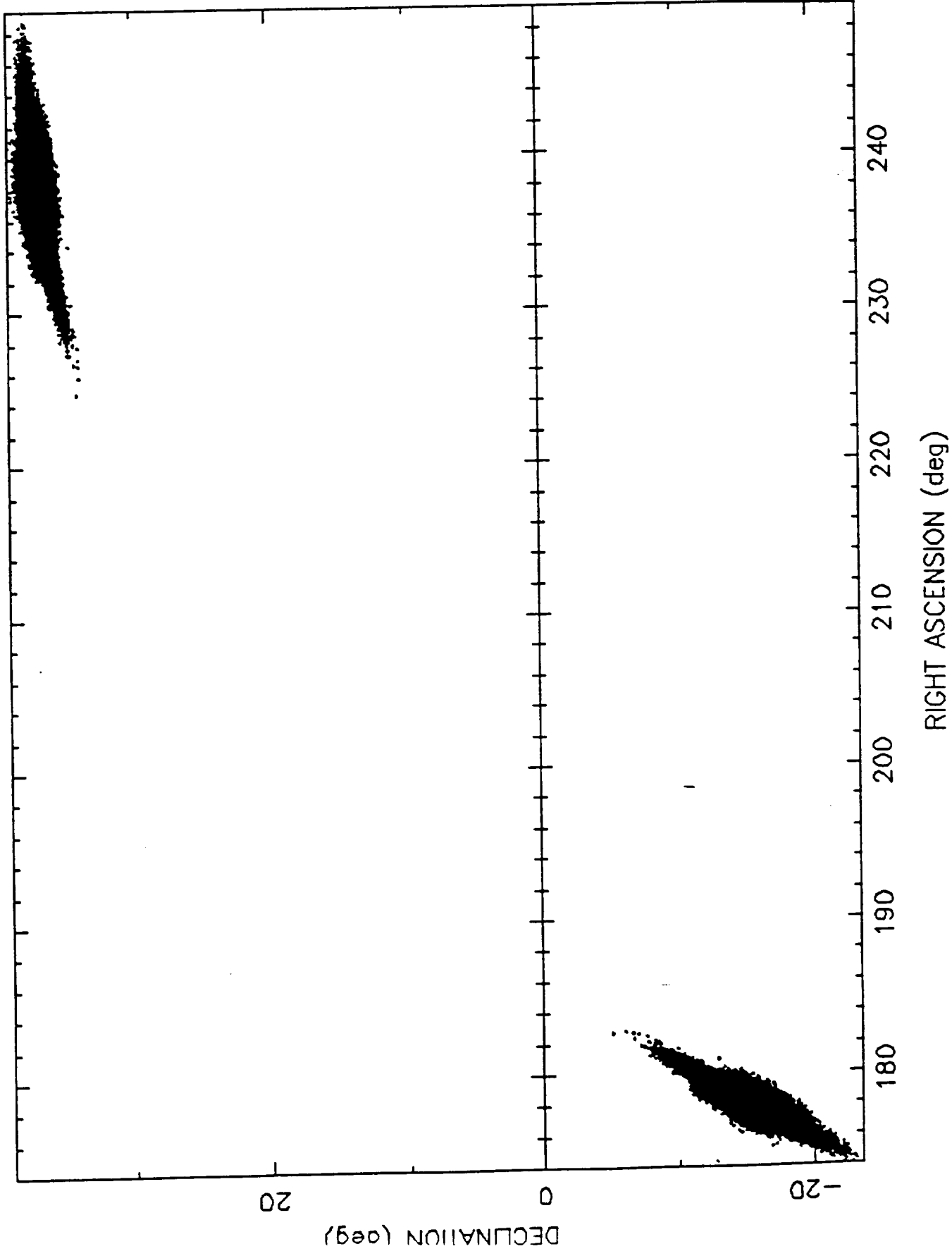
B781019

B781019
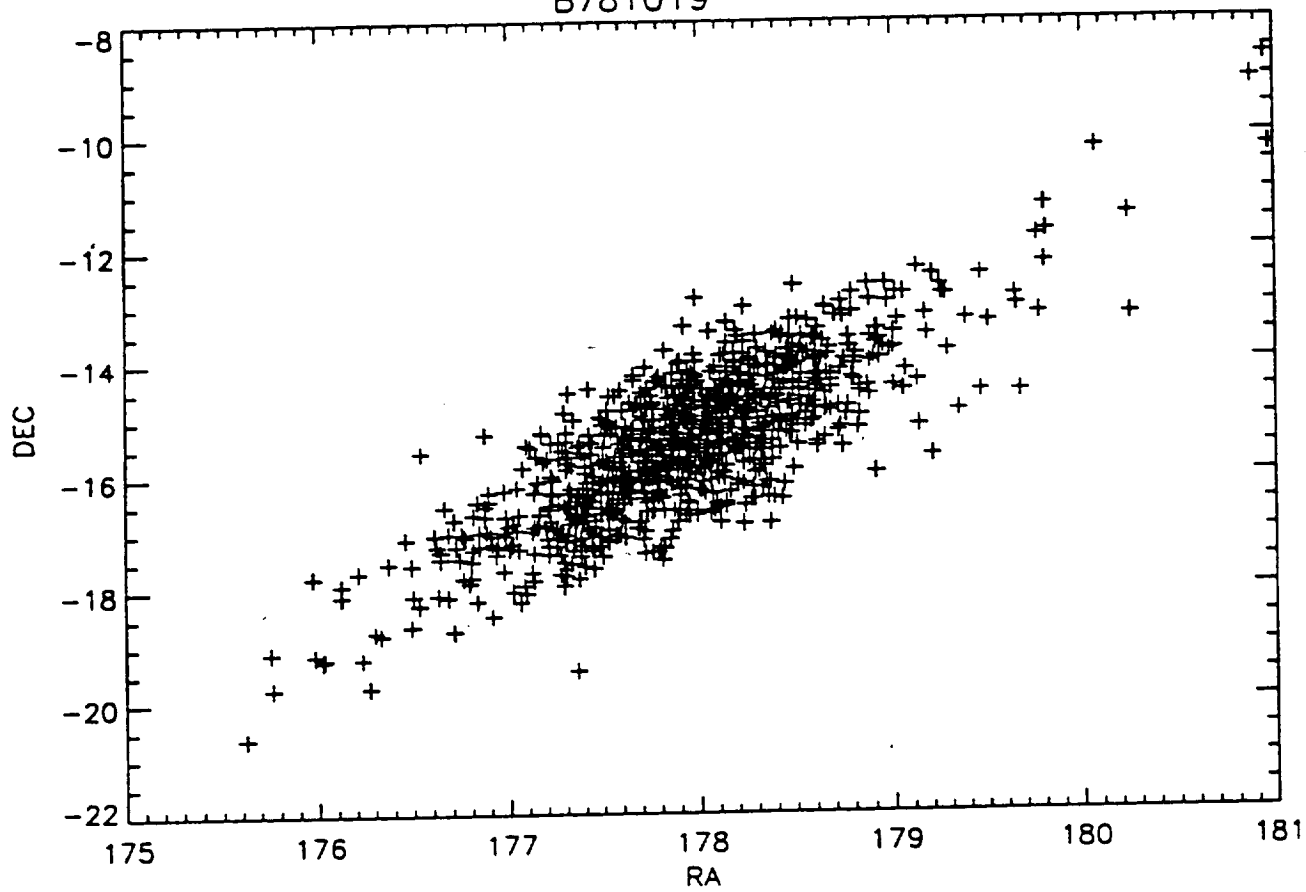
B781023

B781025

B781026

RIGHT ASCENSION (deg)
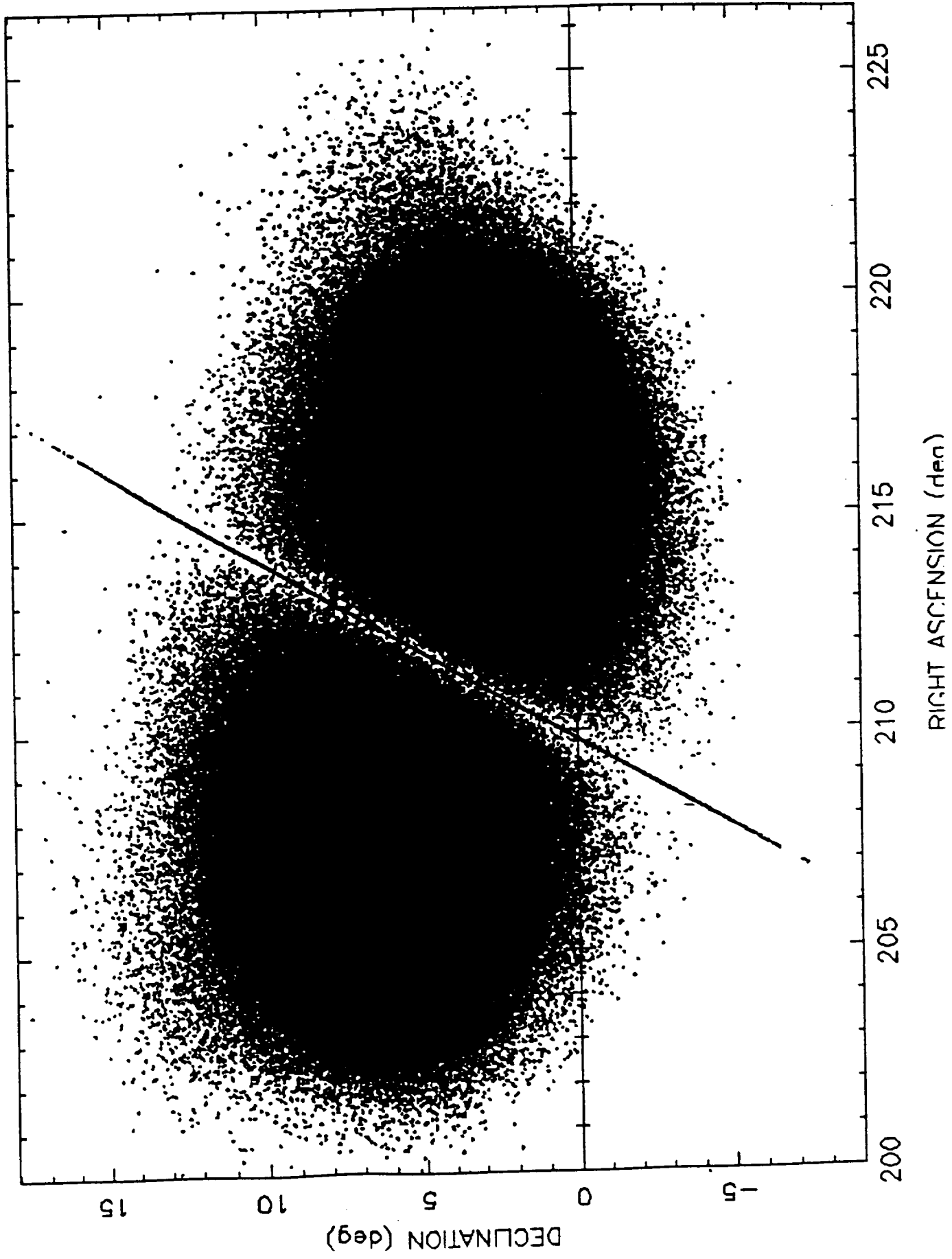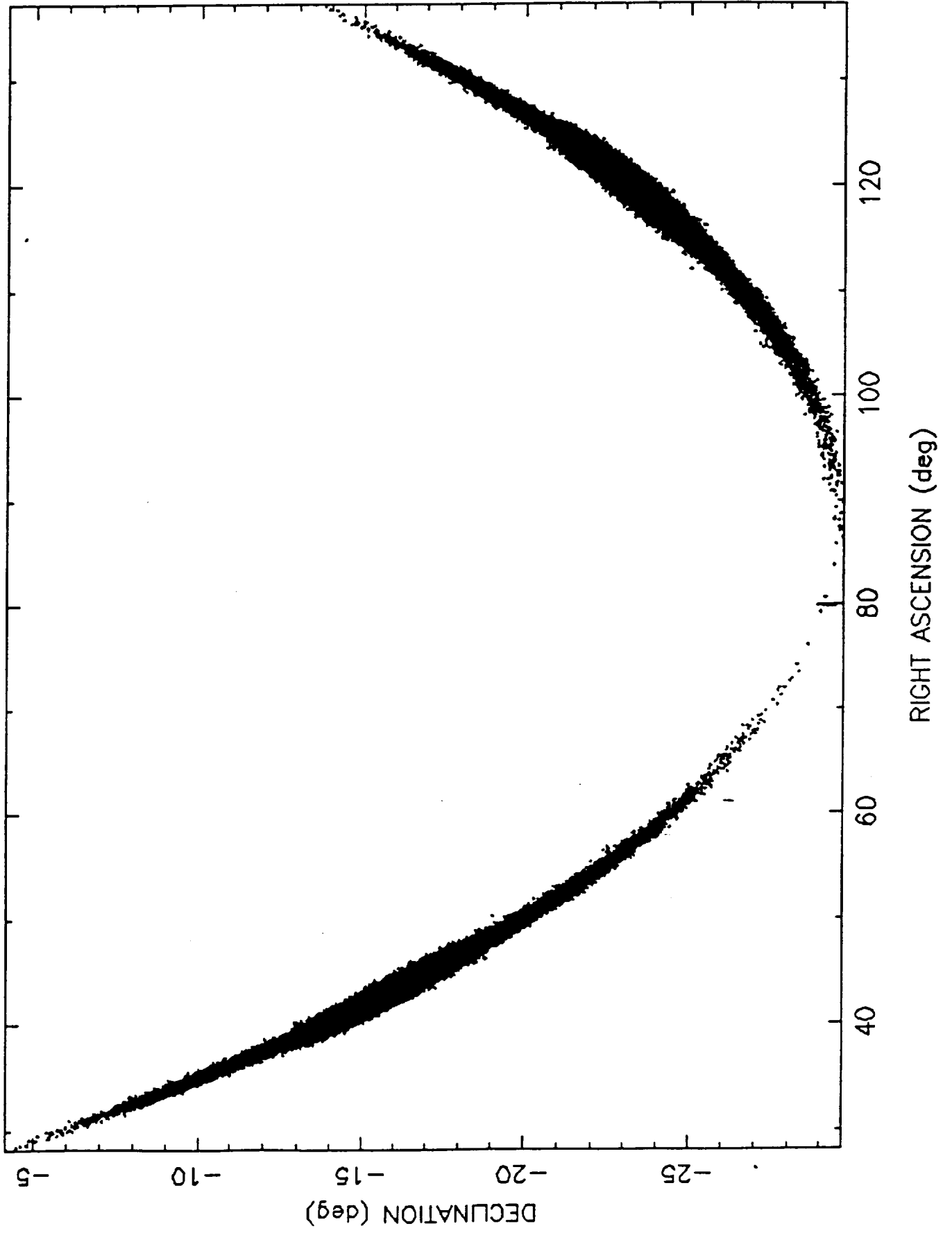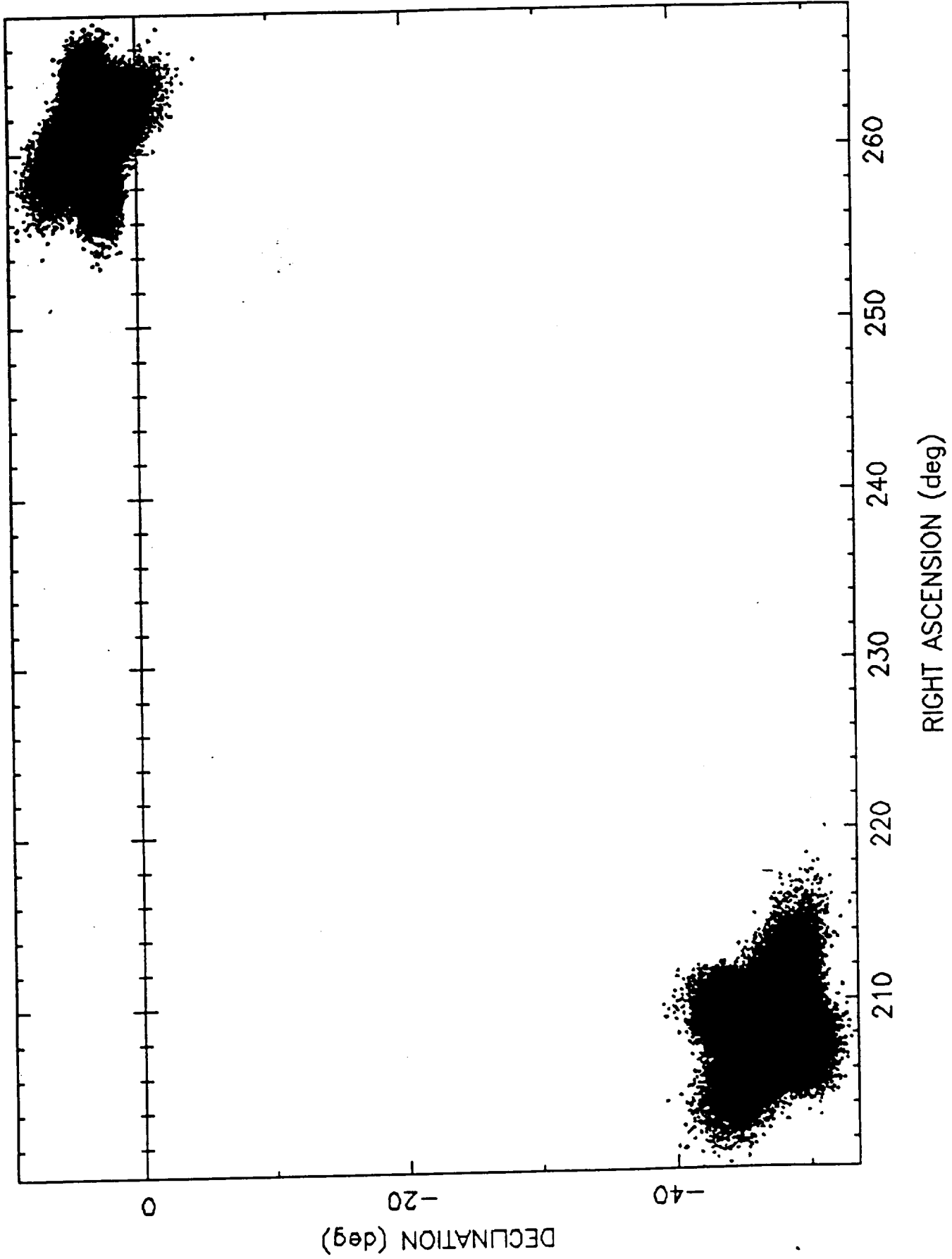
DECLINATION (deg)

B781102A
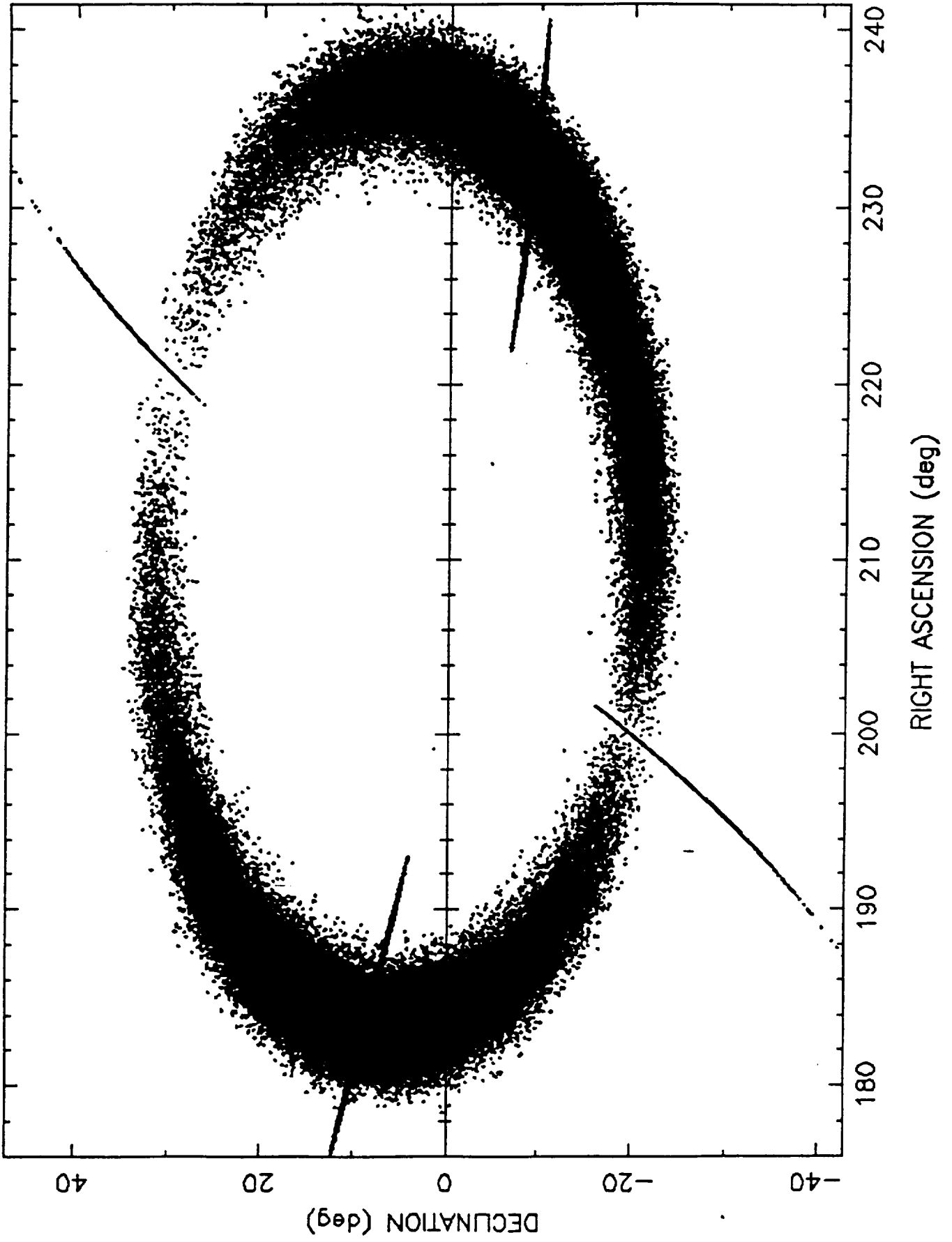
B781115.A

B781115.A

RIGHT ASCENSION (deg)

DECLINATION (deg)

B781121A

B781217

RIGHT ASCENSION (deg)

B790101

RIGHT ASCENSION (deg)

B790105.

DECLINATION (deg)

RIGHT ASCENSION (deg)

B790107

RIGHT ASCENSION (deg)
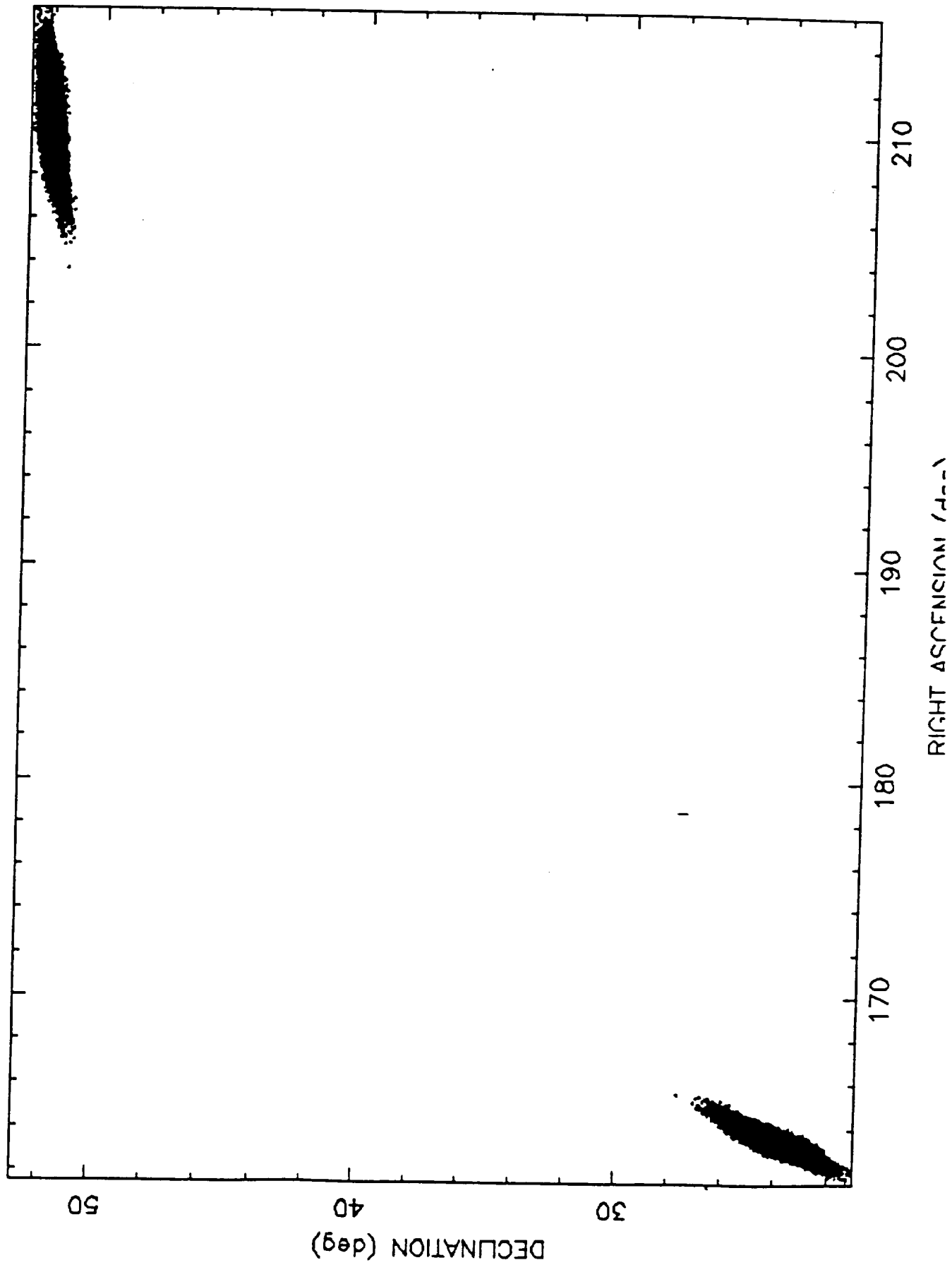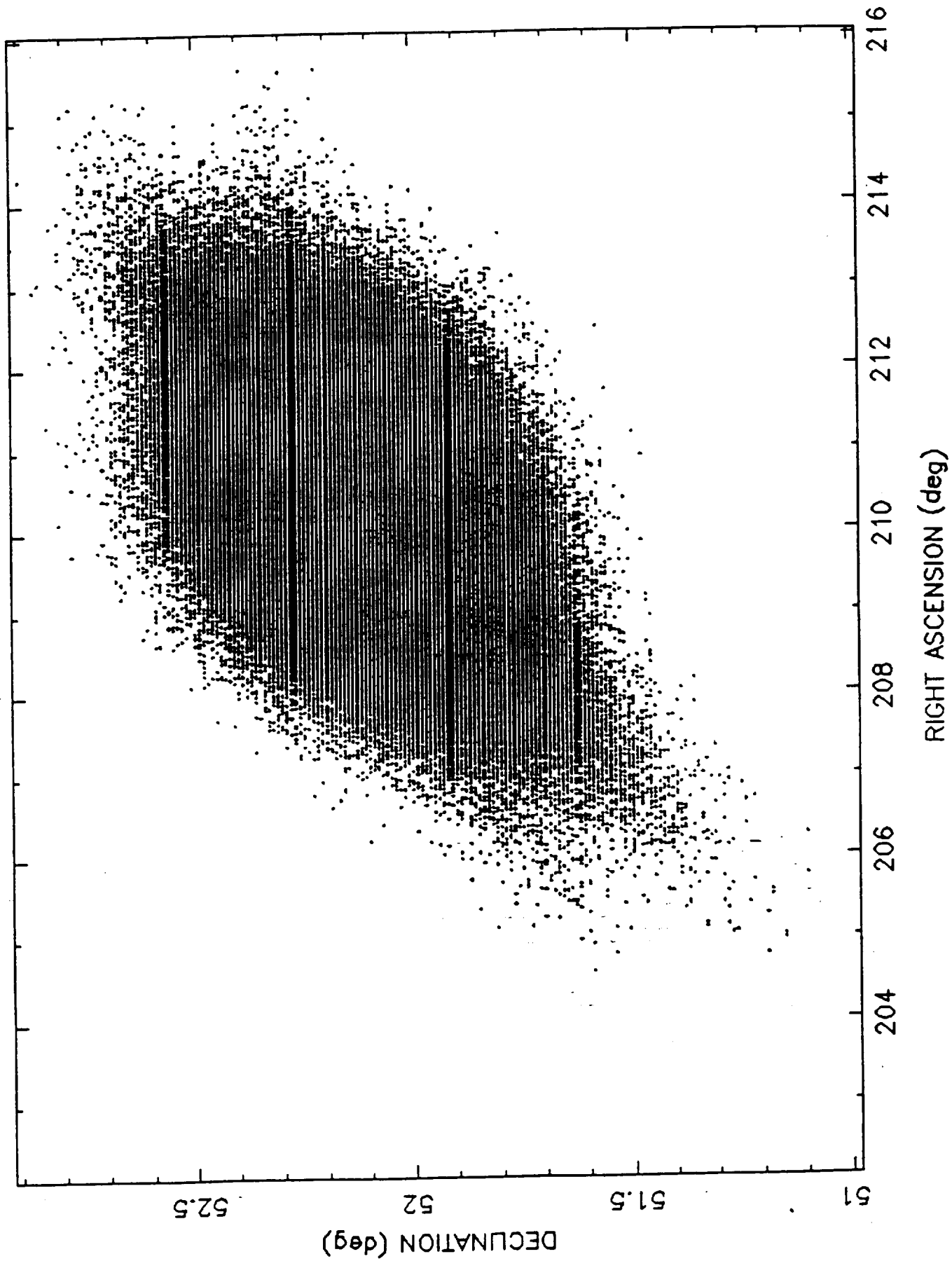
DECLINATION (deg)
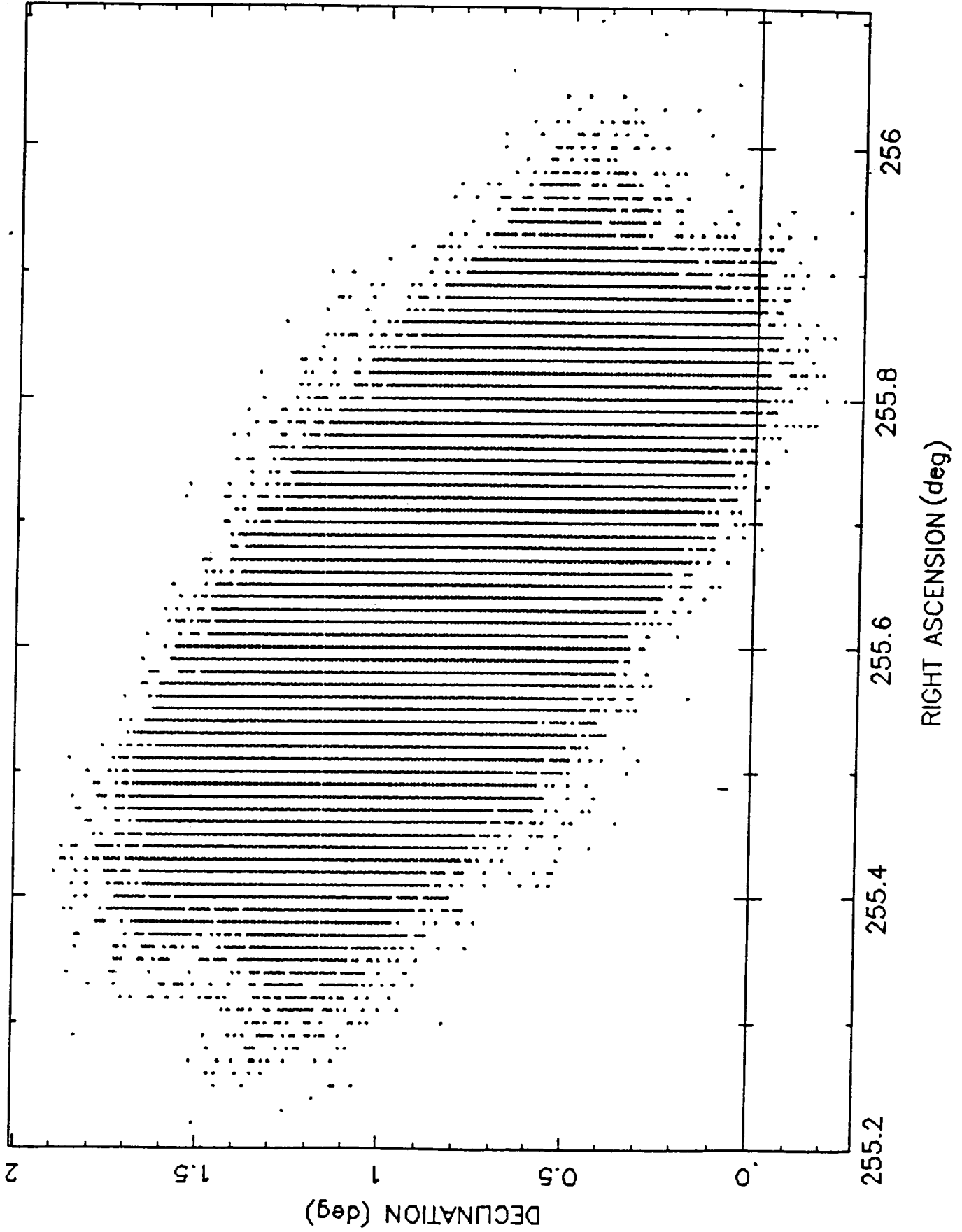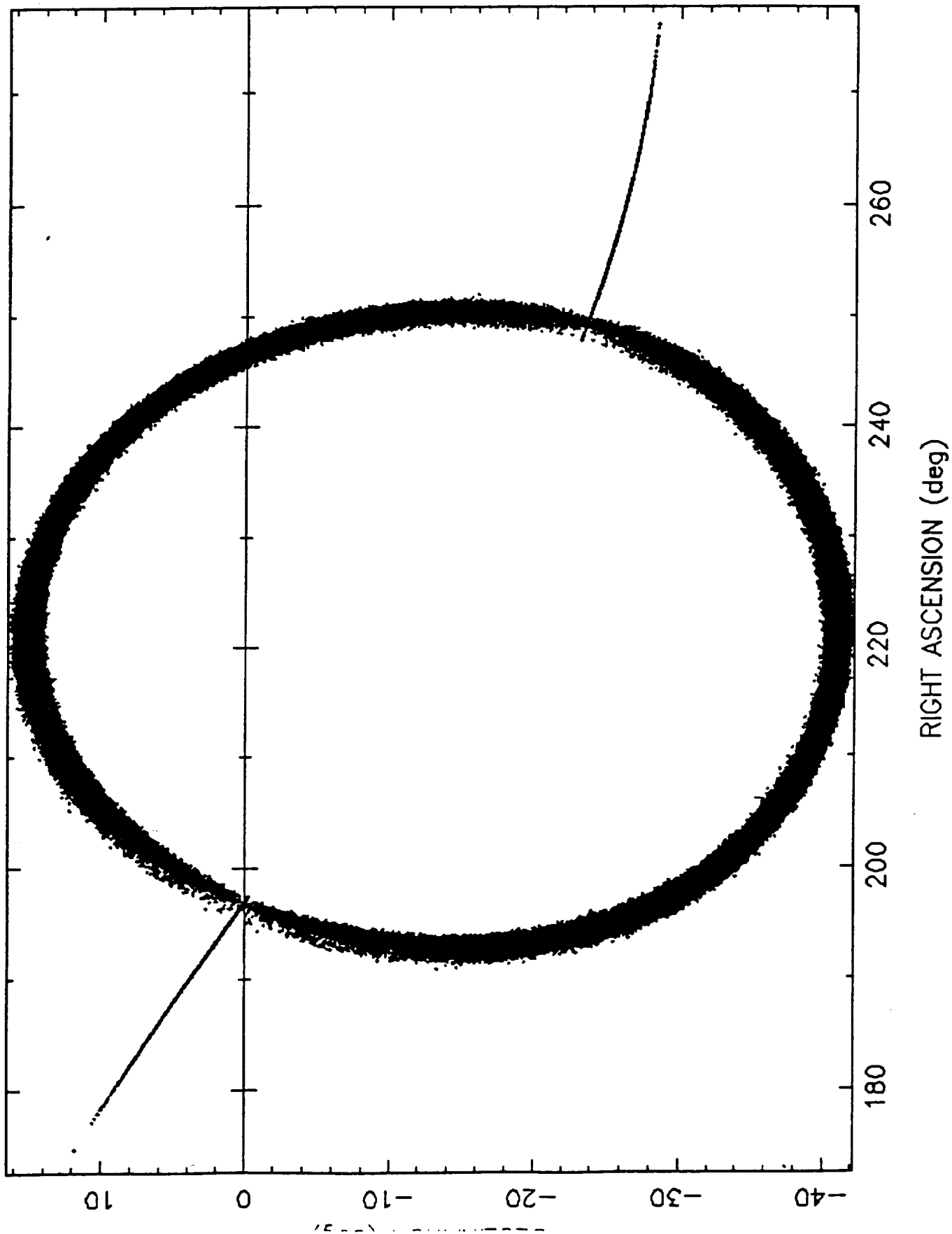
B790116
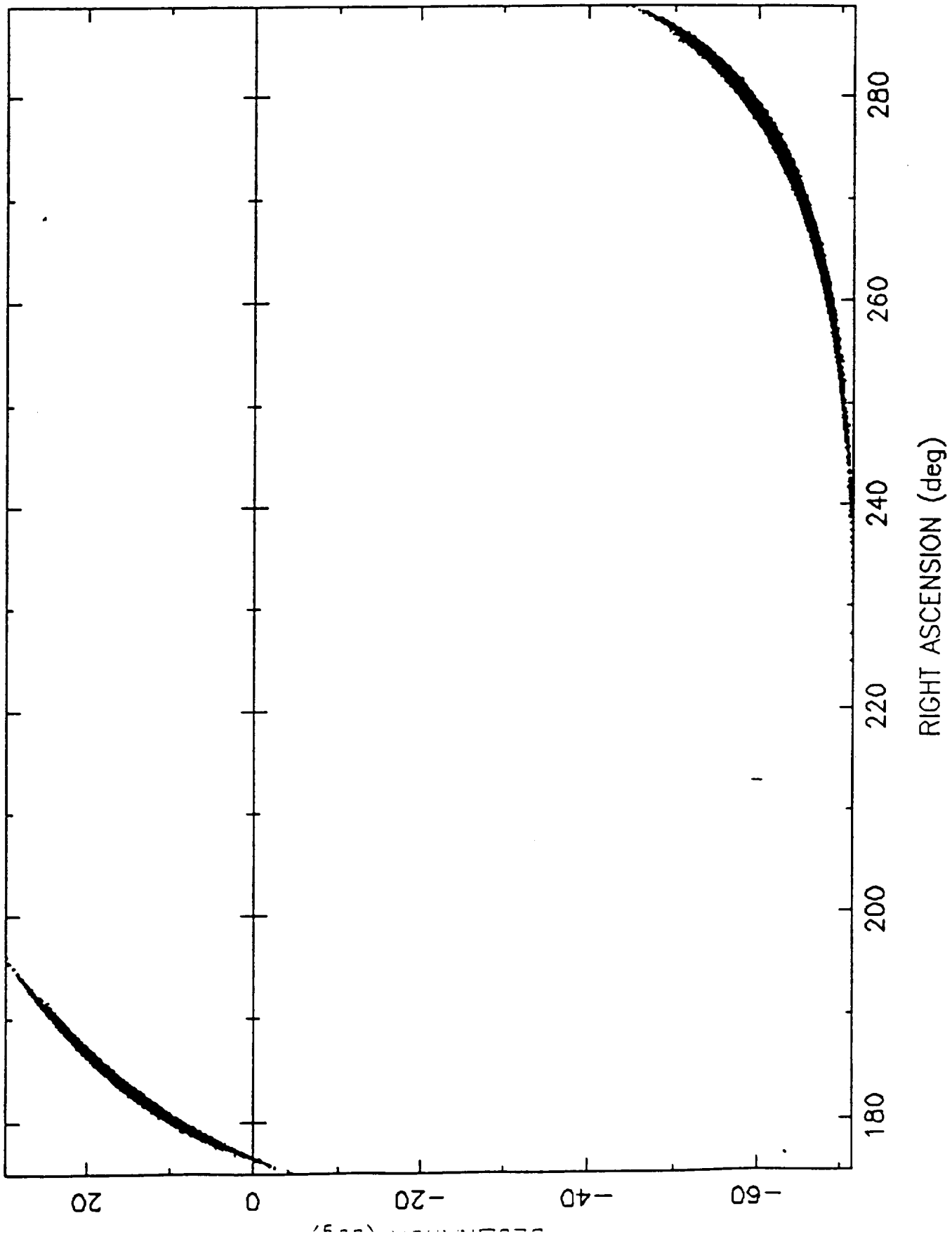
DECLINATION (deg)
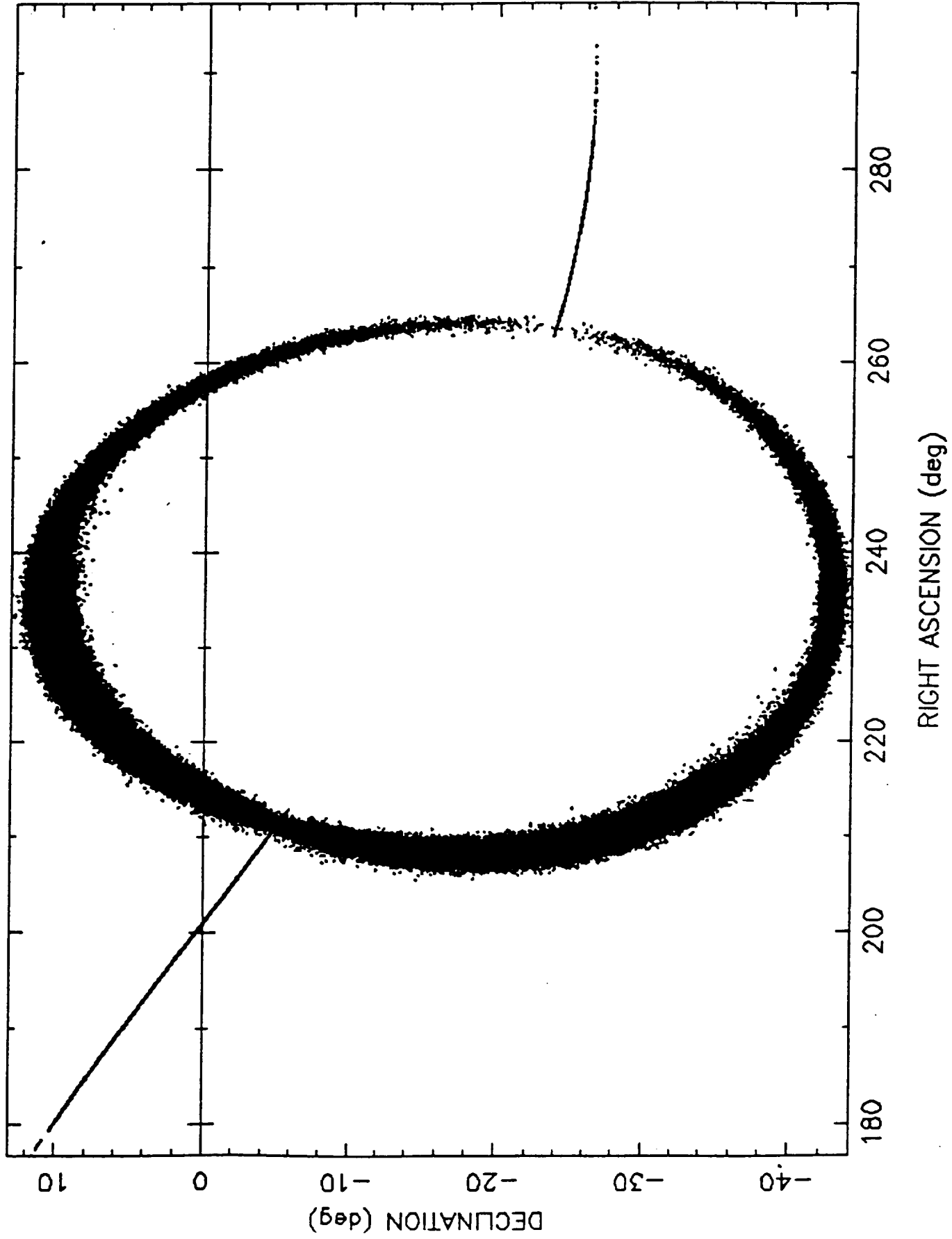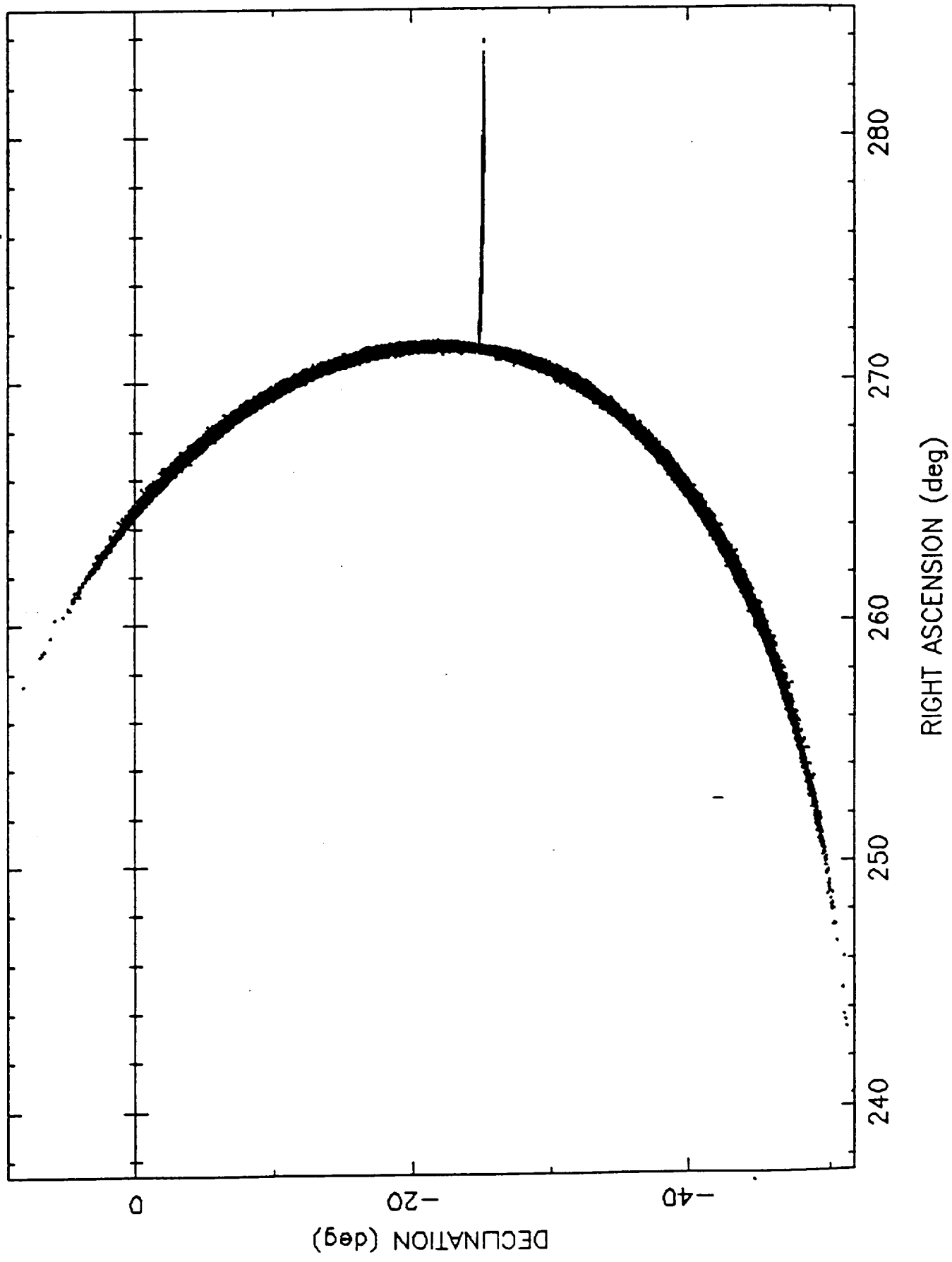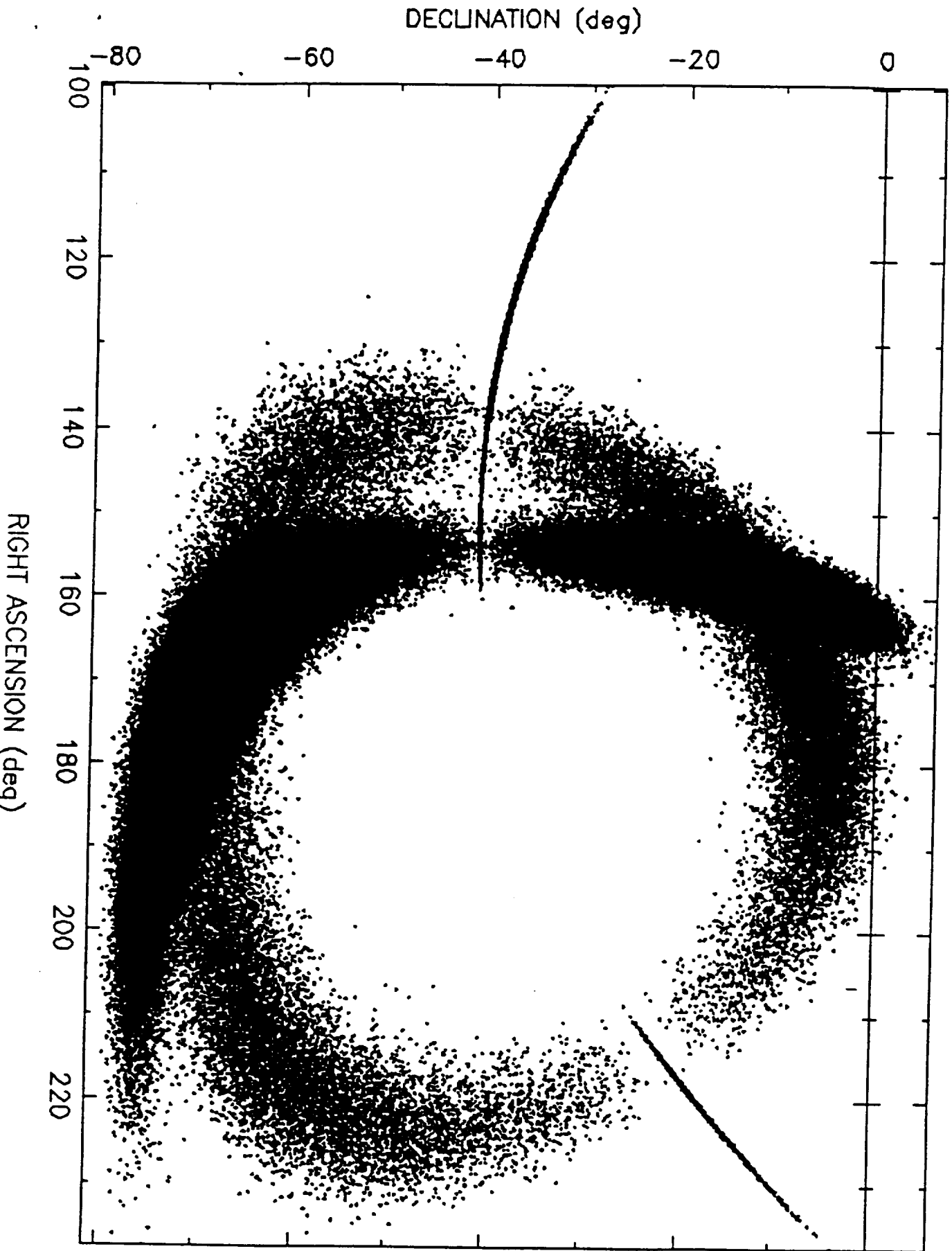
RIGHT ASCENSION (deg)
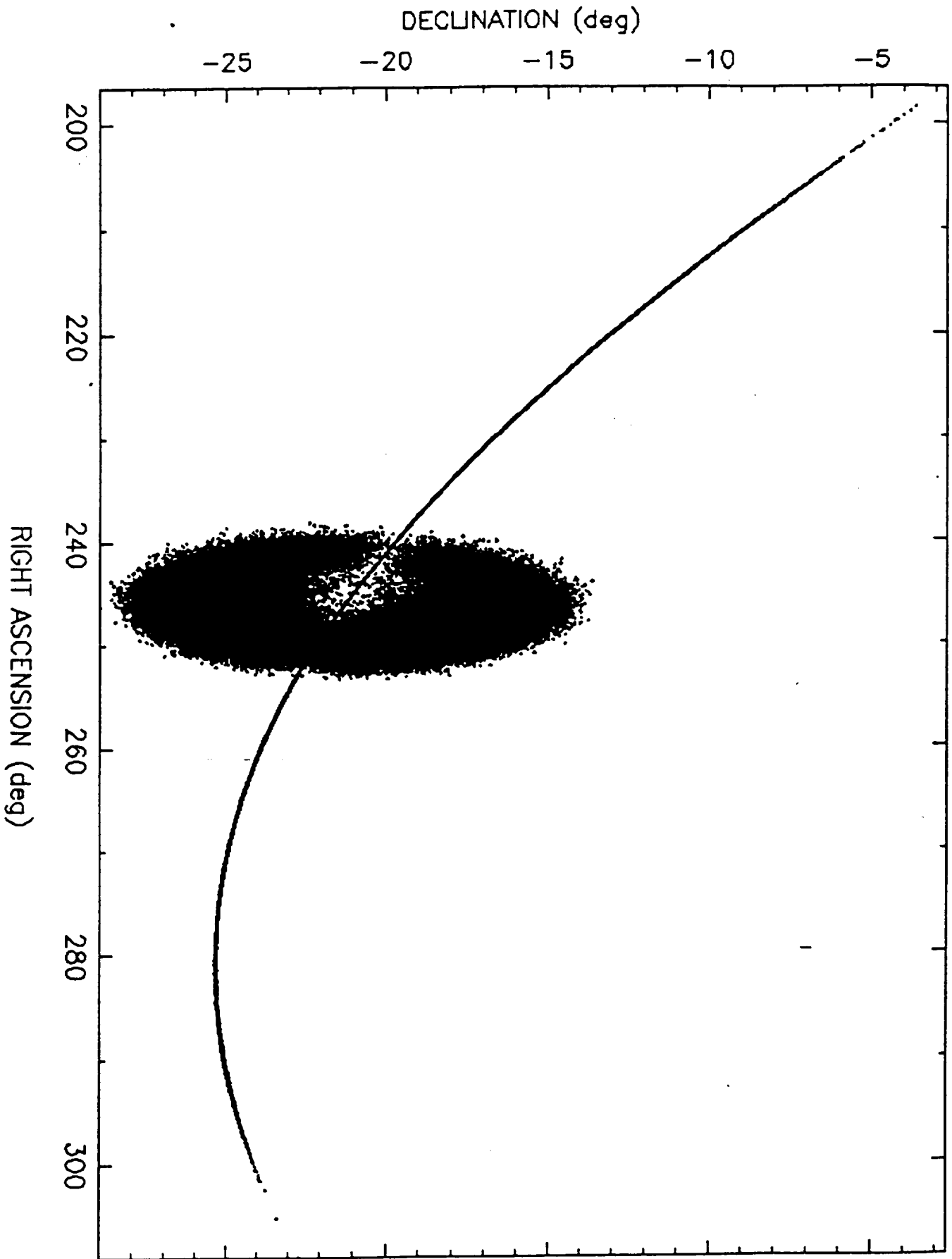
B790119

DECLINATION (deg)

B790208

B790213

B790305.A

B790327.B

DECLINATION (deg)

RIGHT ASCENSION (deg)

B790402.B

B790412.B

B790419

B790504

B790504 :
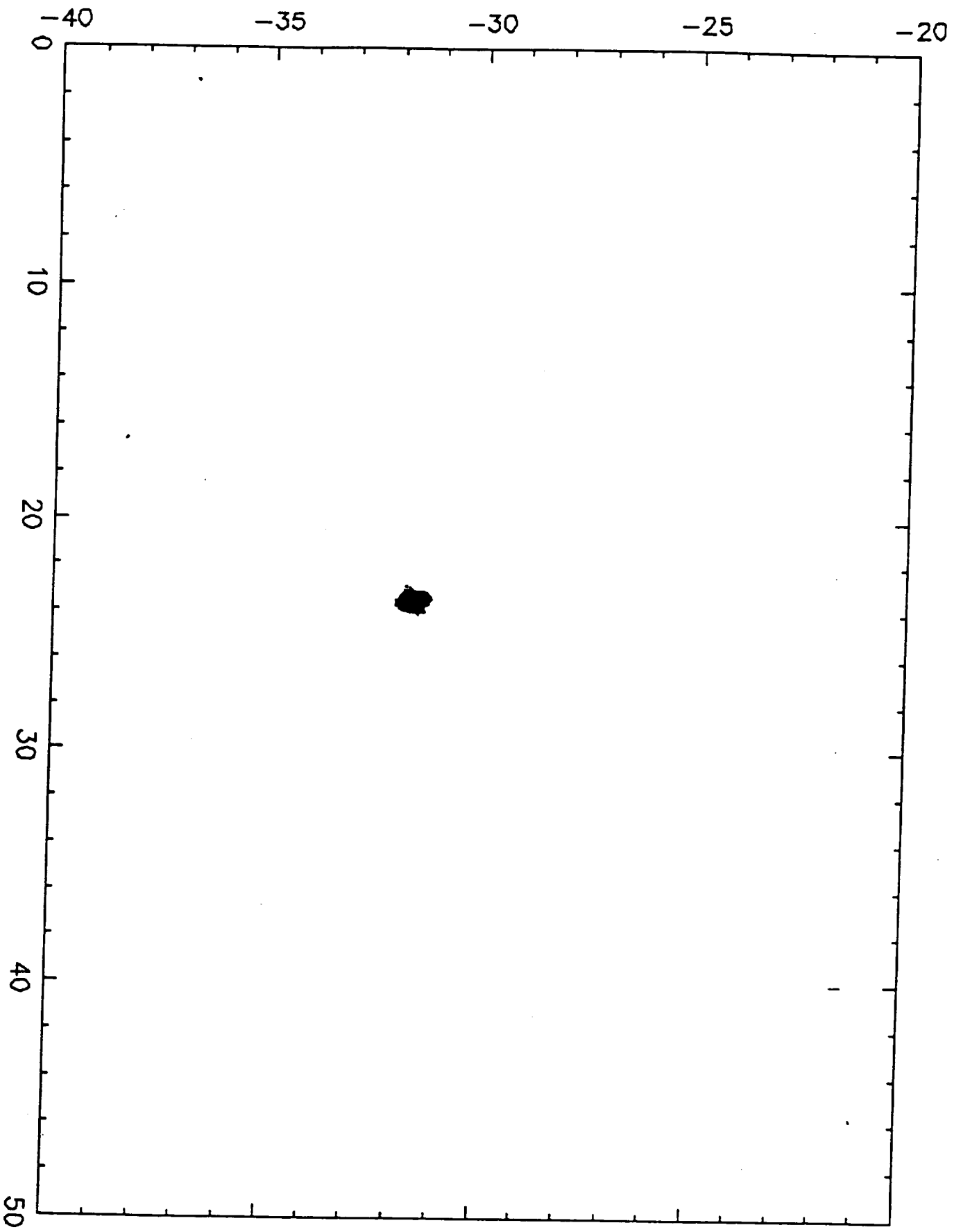
DECLINATION (deg)

RIGHT ASCENSION (deg)

B790514
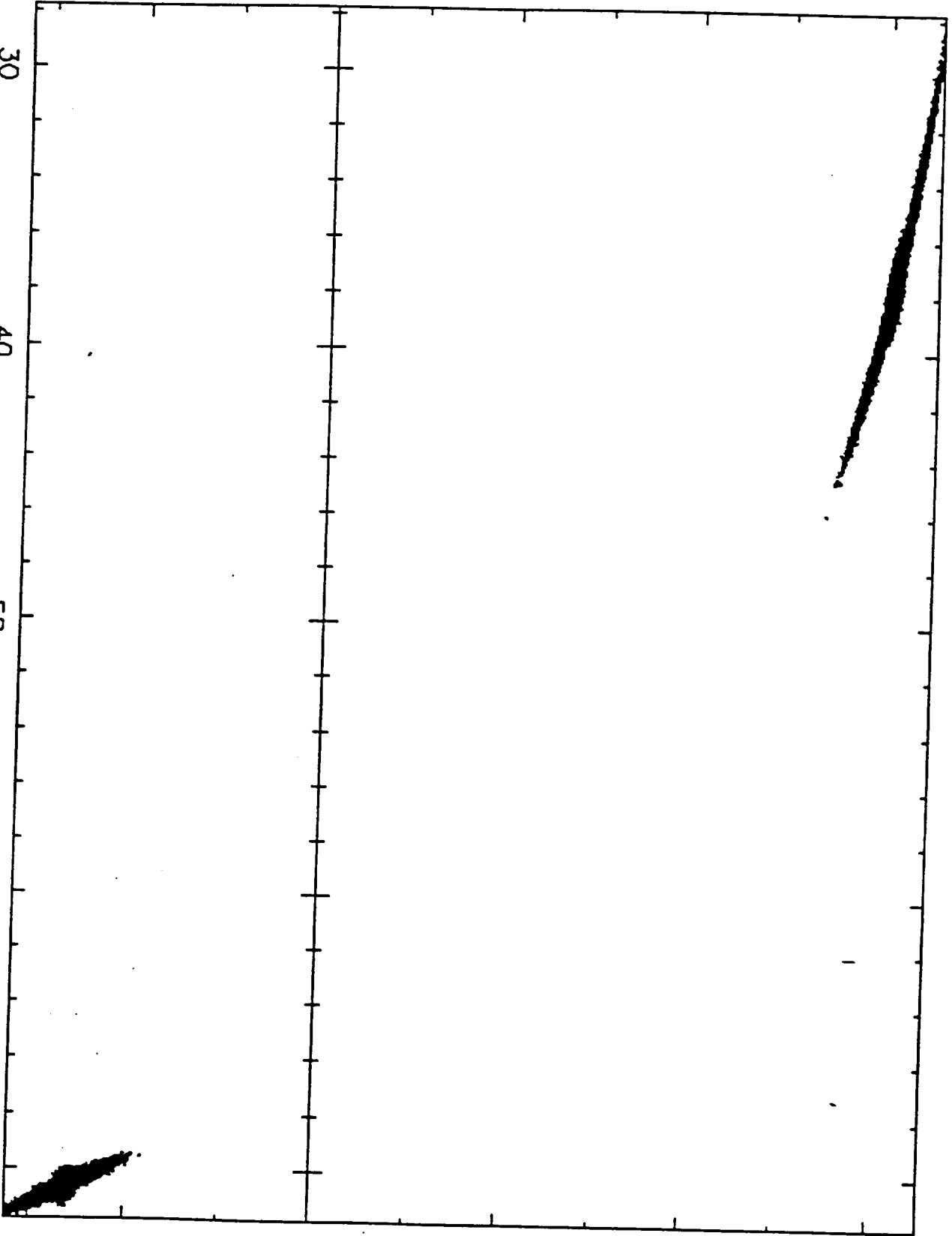
DECLINATION (deg)

-40   -30   -20   -10   0

312

314

316

318

320

322

324

B790622.B

B790731

DECLINATION (deg)

RIGHT ASCENSION (deg)

B790929

DECLINATION (deg)
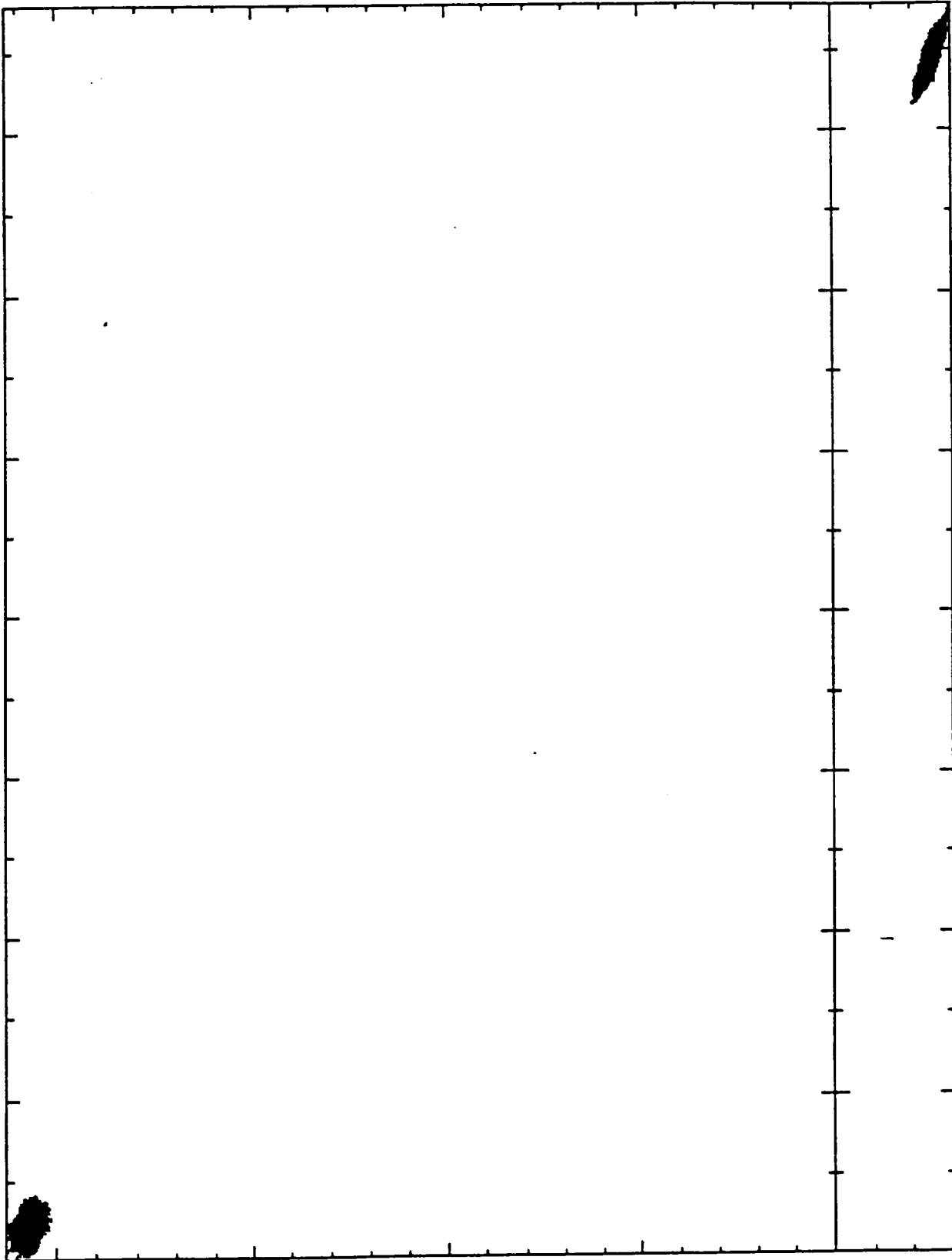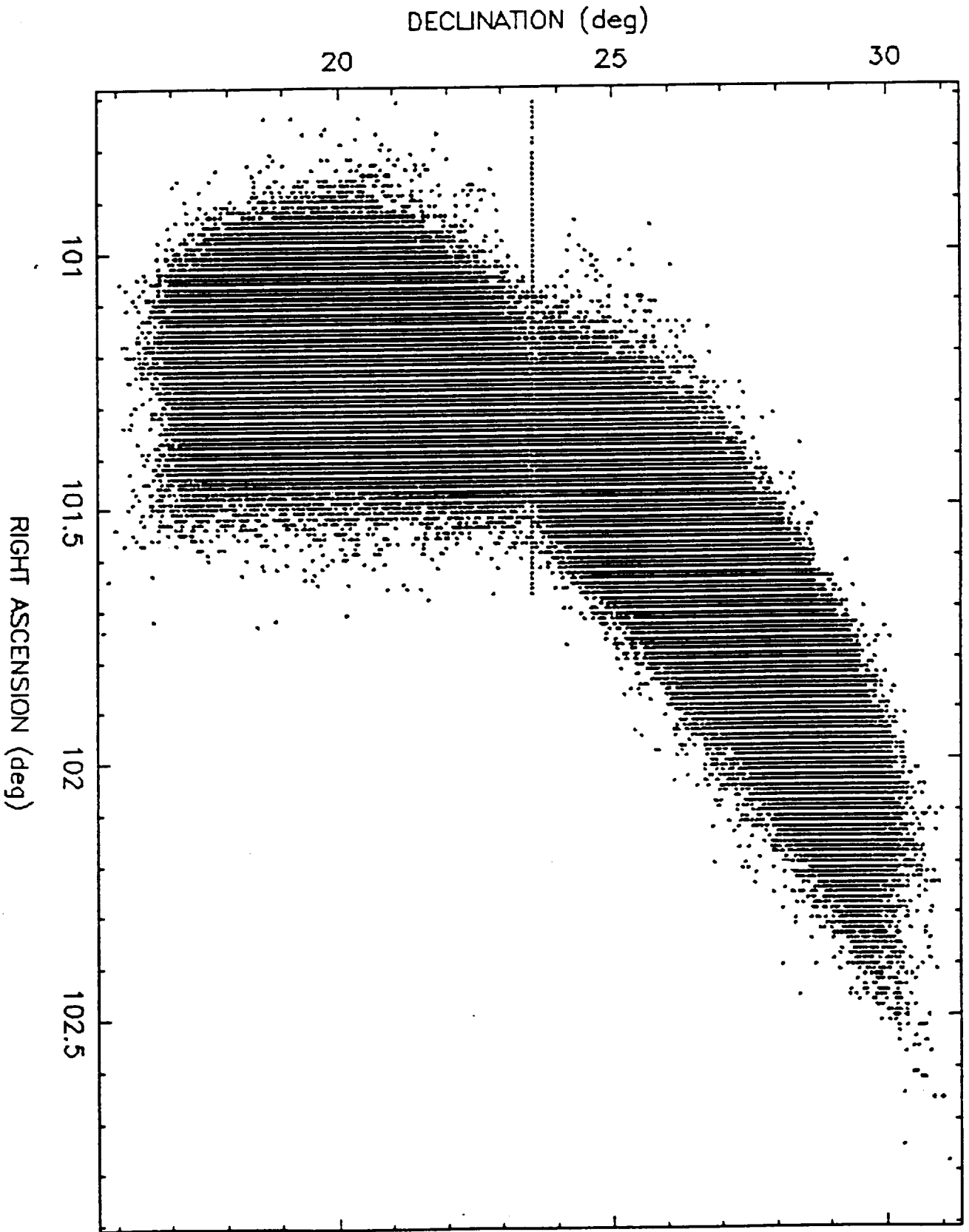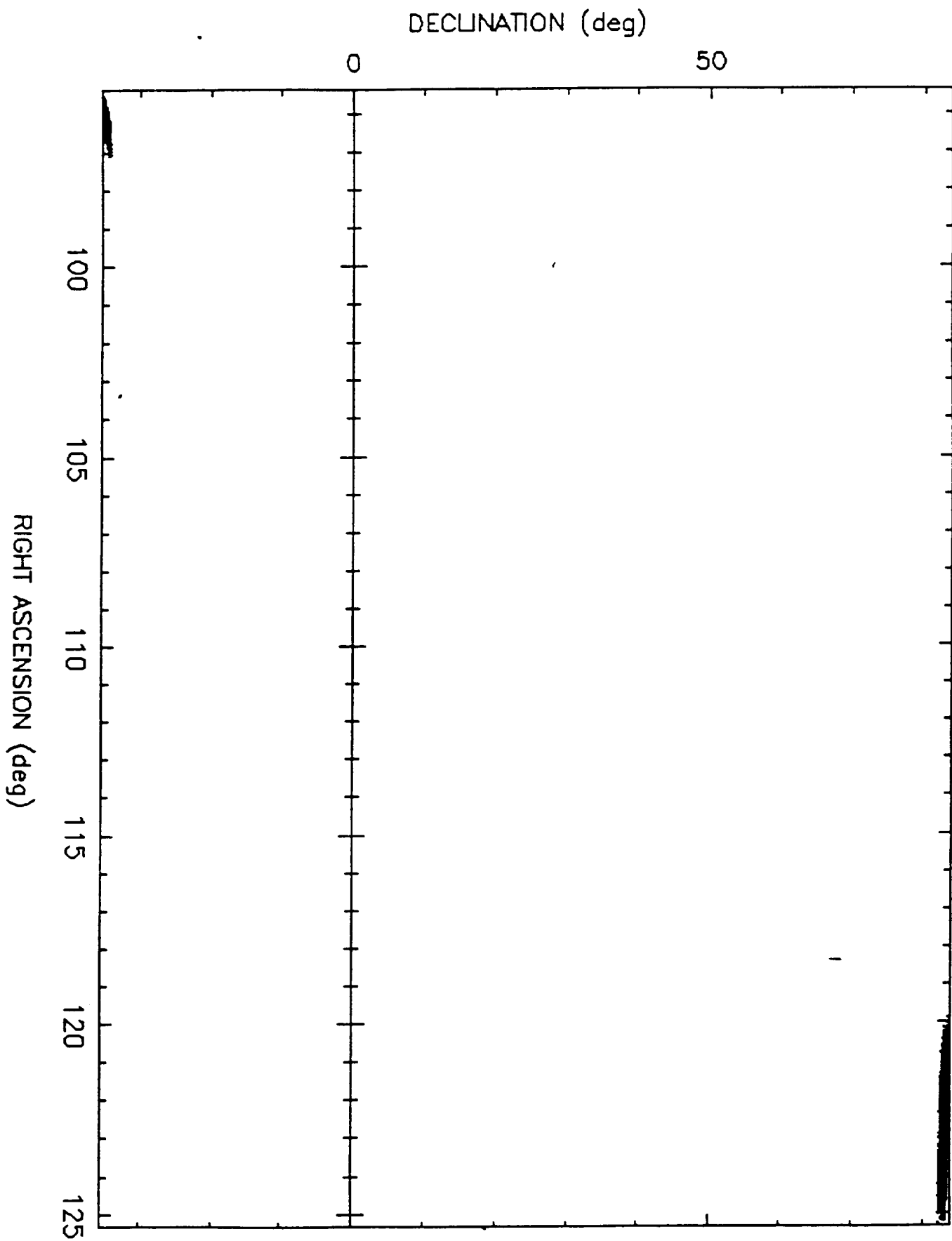
RIGHT ASCENSION (deg)

B791014

DECLINATION (deg)

B791018.
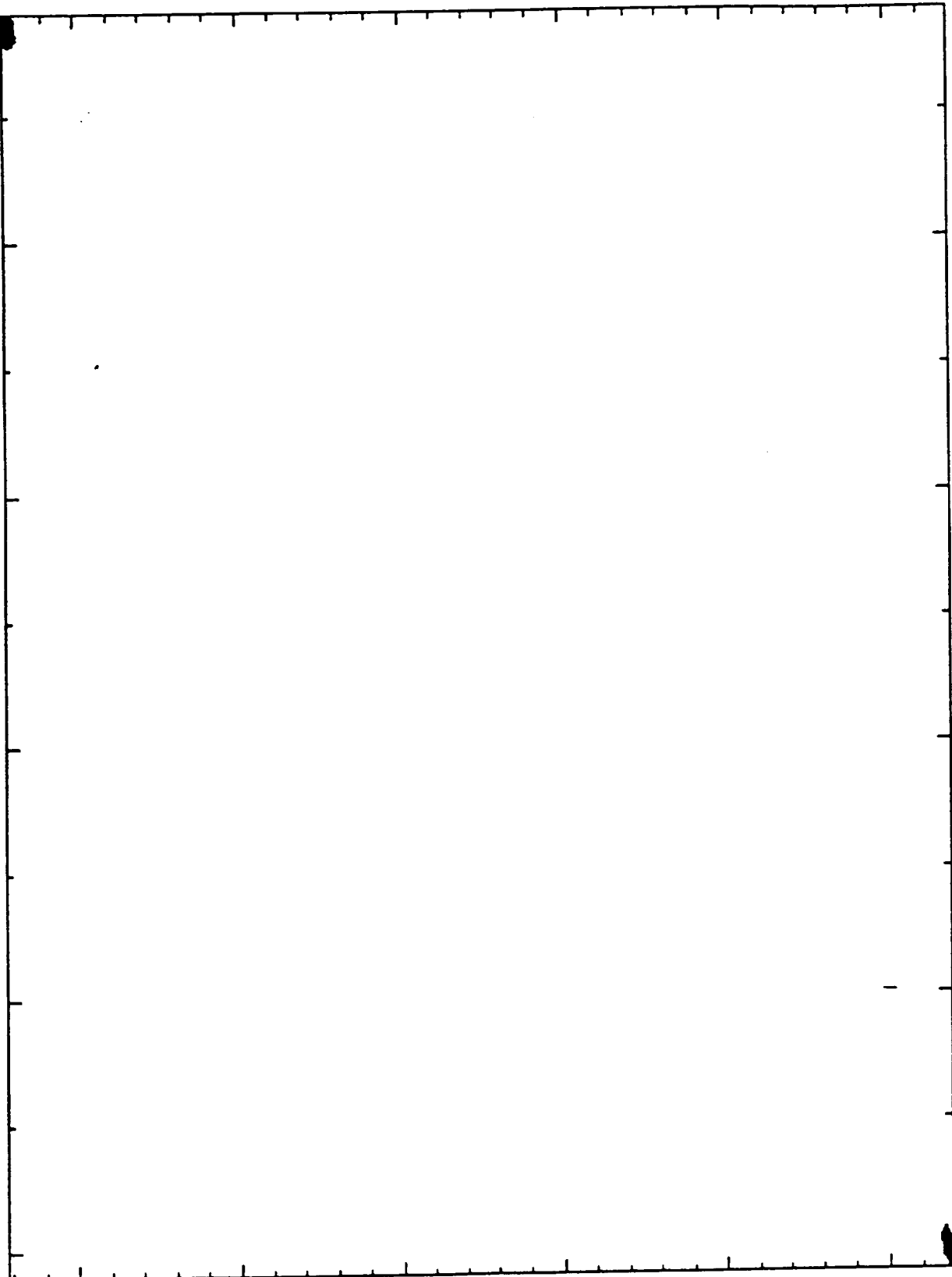
DECLINATION (deg)

B791031A

DECLINATION (deg)

RIGHT ASCENSION (deg)

B791101

DECLINATION (deg)

B791101

DECLINATION (deg)

B791105

DECLINATION (deg)

RIGHT ASCENSION (deg)

B791111

DECLINATION (deg)

RIGHT ASCENSION (deg)

B791115

B791215

DECLINATION (deg)

-50   0   50

B791220.A

RIGHT ASCENSION (deg)

100   150   200   250   300

DECLINATION (deg)

RIGHT ASCENSION (deg)

B791222A

DECLINATION (deg)

-20   0   20

RIGHT ASCENSION (deg)

50   100   150   200   250   300   350

B800103.A

B800105

B800116

DECLINATION (deg)

RIGHT ASCENSION (deg)

B800213